



Seawater $^{87}\text{Sr}/^{86}\text{Sr}$ ratios along continental margins: Patterns and processes in open and restricted shelf domains

Sofia El Meknassi, Guillaume Dera, Marc de Rafélis, Chloé Brahmi, Franck Lartaud, Florent Hodel, Catherine Jeandel, Ludovic Menjot, Stéphanie Mounic, Manuel Henry, et al.

► To cite this version:

Sofia El Meknassi, Guillaume Dera, Marc de Rafélis, Chloé Brahmi, Franck Lartaud, et al.. Seawater $^{87}\text{Sr}/^{86}\text{Sr}$ ratios along continental margins: Patterns and processes in open and restricted shelf domains. *Chemical Geology*, 2020, 558, pp.119874. 10.1016/j.chemgeo.2020.119874 . hal-03038469

HAL Id: hal-03038469

<https://hal.science/hal-03038469>

Submitted on 21 Sep 2022

HAL is a multi-disciplinary open access archive for the deposit and dissemination of scientific research documents, whether they are published or not. The documents may come from teaching and research institutions in France or abroad, or from public or private research centers.

L'archive ouverte pluridisciplinaire **HAL**, est destinée au dépôt et à la diffusion de documents scientifiques de niveau recherche, publiés ou non, émanant des établissements d'enseignement et de recherche français ou étrangers, des laboratoires publics ou privés.



Distributed under a Creative Commons Attribution - NonCommercial 4.0 International License

Seawater $^{87}\text{Sr}/^{86}\text{Sr}$ ratios along continental margins: patterns and processes in open and restricted shelf domains

Sofia El Meknassi¹, Guillaume Dera^{1*}, Marc De Rafélis¹, Chloé Brahmi³, Franck Lartaud², Florent Hodel¹, Catherine Jeandel⁴, Ludovic Menjot¹, Stéphanie Mounic¹, Manuel Henry¹, Philippe Besson¹, Valérie Chavagnac¹

¹ Géosciences Environnement Toulouse (GET), Université Paul Sabatier Toulouse 3, CNRS UMR 5563, IRD, Toulouse, France

² Sorbonne Université, CNRS UMR 8222, Laboratoire d'Ecogéochimie des Environnements Benthiques (LECOB), Observatoire Océanologique de Banyuls, Banyuls-sur-Mer, France

³ Université de la Polynésie Française, UMR 241 Ecosystèmes Insulaires Océaniques (EIO), Faa'a – Tahiti, French Polynesia

⁴ Laboratoire d'Etudes en Géophysique et Océanographie Spatiales (LEGOS), Université Paul Sabatier Toulouse 3, CNRS UMR 5566, IRD, Toulouse, France

*Corresponding author: guillaume.dera@get.omp.eu

Highlights:

- Homogeneous $^{87}\text{Sr}/^{86}\text{Sr}$ ratios similar to the oceanic value in open shelf contexts
- Noticeable heterogeneity of $^{87}\text{Sr}/^{86}\text{Sr}$ ratios in lagoons and epeiric seas
- Importance of submarine groundwater discharges which may locally supply 10 to 60% of Sr in lagoons
- Oceanic Sr inputs and $^{87}\text{Sr}/^{86}\text{Sr}$ homogenization controlled by the coastal morphology

Abstract

To better constrain the Sr isotope budget in marginal domains without any fluvial inputs, we analyzed the chemical composition and $^{87}\text{Sr}/^{86}\text{Sr}$ ratio of waters and shells from four locations: two coastal lagoons, one hemipelagic platform and one open marine shelf. Our results highlight homogeneous $^{87}\text{Sr}/^{86}\text{Sr}$ ratios typical of oligotrophic oceanic waters (OOW) (i.e., 0.709172 ± 0.000023) in the Pacific Tatakoto atoll and along a Mediterranean shore to offshore transect (~25km off Banyuls-sur-Mer, BSM). This attests that oceanic inputs from oligotrophic areas remain the main Sr source in open shelf areas compared with submarine groundwater discharges (SGD) or particulate dissolution influences. In BSM, only foreshore data are more radiogenic, possibly due to rainwater mixing, local groundwater springs or more efficient particle dissolution in the intertidal zone. In restricted areas, we report variable $^{87}\text{Sr}/^{86}\text{Sr}$ ratios between the Salses-Leucate (France) and Oualidia (Morocco) lagoons. The first one has homogeneous $^{87}\text{Sr}/^{86}\text{Sr}$ ratio typical of OOW except close to groundwater discharges. In Oualidia, $^{87}\text{Sr}/^{86}\text{Sr}$ ratios decrease by 1.2×10^{-3} from OOW values close to the Atlantic inlet to progressively less radiogenic ones upstream within the interior of the lagoon. These differences depend on several factors including the leaky, restricted or choked morphology of lagoons modulating the oceanic Sr inputs, but also SGD fluxes whose $^{87}\text{Sr}/^{86}\text{Sr}$ ratios and Sr concentrations are highly variable according to the nature of rocks leached in karstic aquifer. In Oualidia, the low $^{87}\text{Sr}/^{86}\text{Sr}$ ratios correspond to high Sr concentrations (up to $150 \mu\text{mol}\cdot\text{l}^{-1}$) issued from the dissolution of Mesozoic evaporites, leading to SGD fluxes accounting for 60% of the local Sr budget. Through data compilation, we show that similar $^{87}\text{Sr}/^{86}\text{Sr}$ gradients and processes prevail at the whole Mediterranean scale. Finally, we postulate that high coastal water retention times can also account for anomalous coastal $^{87}\text{Sr}/^{86}\text{Sr}$ ratios and that the combination of water mass restriction, SGD, bioadsorption and early diagenetic processes could decrease seawater Sr concentrations in some marginal areas.

1. Introduction

Although the strontium isotope compositions ($^{87}\text{Sr}/^{86}\text{Sr}$) of river waters and submarine hydrothermal sources strongly vary across the globe (with respective averages of 0.7119 and 0.7037; Palmer and Edmond, 1989; 1992; Bach and Humphris, 1999; Davis et al., 2003; Pearce et al., 2015; Chavagnac et al., 2018), the $^{87}\text{Sr}/^{86}\text{Sr}$ of oligotrophic oceanic waters (OOW) remains homogeneous worldwide at 0.709172 ± 0.000023 (see El Meknassi et al., 2018 for a recent synthesis). This paradigm is due to the long residence time of Sr in the ocean (i.e., ~ 2.5 Myr; Hodell et al., 1990) compared to the global ocean mixing duration ranging from 1000 to 2000 years (DeVries and Primeau, 2011). However, the OOW $^{87}\text{Sr}/^{86}\text{Sr}$ ratios fluctuated markedly through the Phanerozoic, as reported from Sr isotope data of fossil archives (Peterman et al., 1970; Burke et al., 1982; Veizer, 1989; Zaky et al., 2018). These secular variations are ascribed either to global geodynamic events modulating the respective contribution of terrestrial (radiogenic) and hydrothermal (unradiogenic) Sr sources to oceans or to paleogeographic and climatic changes modifying the continental weathering of rocks of different age and lithology (Reeder et al., 1972; Brass, 1976; Goldstein and Jacobsen, 1987; Bataille et al., 2017; Peucker-Ehrenbrink and Fiske, 2019). By assuming a homogeneous OOW $^{87}\text{Sr}/^{86}\text{Sr}$ ratio at a global scale, these long-term $^{87}\text{Sr}/^{86}\text{Sr}$ variations are thus widely used for dating sedimentary series through chemostratigraphic calibration of new fossil data (McArthur, 1994; McArthur et al., 2012) or testing paleogeographic and climatic hypotheses (Godd  ris et al., 2017).

Despite the popularity of this paleoenvironmental proxy, the question of whether fossil carbonate shells may be used to reconstruct past OOW $^{87}\text{Sr}/^{86}\text{Sr}$ fluctuations is still a matter of debate as most of these organisms thrived in epeiric and shelf domains potentially disconnected from the global oceanic Sr reservoir. This is partly supported by the apparent heterogeneity of modern shell and (euhaline to brachyhaline) seawater $^{87}\text{Sr}/^{86}\text{Sr}$ ratios from

worldwide marine shelves, with respective ranges of 0.707636–0.710483 and 0.704638–710648 (precision on measured $^{87}\text{Sr}/^{86}\text{Sr}$ ratio is better than 10^{-5} ; El Meknassi et al., 2018). Significant offsets between well-dated fossil (or bulk carbonate) $^{87}\text{Sr}/^{86}\text{Sr}$ ratios and the Phanerozoic isotope curve are also regularly reported, even in sedimentary facies indicating outer shelf contexts and/or normal marine environments (Cochran et al., 2003; Nieto et al., 2008; Sessa et al., 2012; Wierzbowski et al., 2012; Eidvin et al., 2014; Schildgen et al., 2014; Briard et al., 2020). While potential analytical, stratigraphical and diagenetic biases may be discarded (Martin and Scher, 2004; Marcano et al., 2015; Bellefroid et al., 2018; Zaky et al., 2018), these mismatches can indicate that, sporadically, seawater $^{87}\text{Sr}/^{86}\text{Sr}$ ratios of epeiric and shelf domains are not necessarily representative of the global OOW value. In most case, these variations result from dissolved Sr supplies delivered by river waters, with contrasted influences on seawater $^{87}\text{Sr}/^{86}\text{Sr}$ ratios according to their Sr concentrations and isotopic ratios linked to the age and lithology of local bedrocks (Palmer and Edmond, 1989, 1992; Bryant et al., 1995; Peucker-Ehrenbrink et al., 2010). This terrestrial Sr contribution is common in restricted environments like epeiric seas, estuaries, fjords, lagoons, and bays where oceanic influences are more restricted and where $^{87}\text{Sr}/^{86}\text{Sr}$ ratios covary landward with salinity (Andersson et al., 1992; Ingram and Sloan, 1992; Israelson and Buchardt, 1999; Basu et al., 2001; Major et al., 2006; Jones et al., 2014; Beck et al., 2013; Wang and You, 2013; Chakrabarti et al., 2018; Shao et al., 2018). However, this river water influence can remain limited in euhaline marginal contexts as, on average, measurable effects on the seawater $^{87}\text{Sr}/^{86}\text{Sr}$ ratio are not expected to occur if freshwater inputs do not drop salinity below a threshold value of 12 (Bryant et al., 1995). Only 5 % of world river systems have water $^{87}\text{Sr}/^{86}\text{Sr}$ ratios sufficiently different from the OOW value to significantly modify the local seawater $^{87}\text{Sr}/^{86}\text{Sr}$ ratio in euhaline marine environments.

Although poorly documented, seawater and shell $^{87}\text{Sr}/^{86}\text{Sr}$ ratios ranging from 0.70890 to 0.70921 have been yet reported in deep outer shelf domains and lagoons not directly subject to major river supply (Müller et al., 1990a; 1990b; Peckmann et al. 2001; Major et al. 2006; Huang et al., 2011; El Meknassi et al., 2018). This suggests that submarine groundwater discharges (SGD) or strontium released from particulate dissolution have a much stronger impact on the coastal Sr budget than currently expected (Beck et al., 2013; Jones et al., 2014 ; Trezzi et al., 2017). A direct consequence is that, depending on oceanic mixing and water retention times on shelves (i.e., ranging from a couple of days to decades or centuries; Liu et al., 2019), the Sr concentrations and $^{87}\text{Sr}/^{86}\text{Sr}$ of marginal areas, could not always be representative of the global oceanic reservoir. In other words, seawater from open shelves and epeiric domains could record Sr isotope anomalies just through cumulative effects of sporadic terrestrial Sr inputs in coastal sub-reservoirs not sufficiently mixed with the global oceanic reservoir.

Here, we test how submarine groundwater discharges (SGD) and water mass restriction can influence the Sr isotope composition of shelf water devoid of river influences by measuring and comparing the $^{87}\text{Sr}/^{86}\text{Sr}$ ratios of waters and shells from four coastal domains with different levels of connection to the open ocean. These include an open shelf Mediterranean transect, two coastal lagoons influenced by groundwater discharges in the Atlantic and Mediterranean contexts, and a Pacific hemipelagic platform. Through data compilation, our aim is also to better document the worldwide variability of seawater $^{87}\text{Sr}/^{86}\text{Sr}$ ratios in the coastal ocean and to better constrain the environmental processes acting on seawater $^{87}\text{Sr}/^{86}\text{Sr}$ patterns in these transition zones.

2. Geological Setting

The seawater $^{87}\text{Sr}/^{86}\text{Sr}$ ratios of three restricted lagoons exhibiting different geomorphological, hydrogeological, hydrodynamical and climatic conditions is investigated in this study (Fig. 1): 1) The Tatakoto atoll in the eastern Tuamotu Archipelago (French Polynesia) in the southern part of the Pacific Ocean; 2) the Salses-Leucate lagoon (France) in the northwestern Mediterranean domain; and 3) the Oualidia lagoon (Morocco) in the North Atlantic domain. These three sites were chosen because they are under the influence of different littoral or reefal barriers, their water resources are issued from various karstic reservoirs, and they have different waves and tide forcing overprinted by different climatic conditions. To get a comparison with an open shelf domain, sampling was also carried out in the Mediterranean Sea along a 25 km-long transect from the rocky coastline of Banyuls-sur-Mer to the submarine Lacaze-Duthiers Canyon (western part of Gulf of Lion).

2.1. Oualidia Lagoon (Morocco)

Formed around 8000 – 6500 BP (Ballouche and Carruesco, 1986), the Oualidia coastal lagoon is located on the western coast of Morocco (Abda Doukkala region) (Fig. 1A) and belongs to a coastal endorheic basin called the Coastal Sahel of Oualidia. The lagoon is 7 km long, 400 m wide, and 4m water deep during the high tide season (Kaid Rassou et al., 2005). It is organized around a main channel of 180 m wide parallel to the coastline and separated from the Atlantic Ocean by a Plio-Quaternary shoal (Ballouche and Carruesco, 1986). The lagoon is connected to the ocean by two inlets to the south (130 and 70 m wide) (El Khalidi et al., 2011), but recent anthropic developments for salt exploitation and eutrophication prevention along the northern part allowed punctual oceanic inflows (Hilmi et al., 2009). Its hydrodynamic balance is influenced by: 1) Atlantic marine inflows linked to important semi-diurnal tidal dynamics (i.e., average amplitude of 0.97 m and main currents $>1 \text{ m.s}^{-1}$; Hilmi et al., 2005; 2009), 2) submarine groundwater supplies estimated from 0.2 to $1.2 \text{ m}^3.\text{s}^{-1}$ (Fakir et

al., 2019), and 3) evaporation rates of 1.3 to 1.5 m.yr⁻¹ characteristic of semi-arid conditions in this region (with precipitation rates of 30 mm.yr⁻¹) (Hilmi et al., 2009). Along seasonal climatic and hydrodynamic conditions, the recurrent groundwater discharge to the lagoon is highlighted by a net salinity gradient ranging from 4 to 36 along a north to south transect (Hilmi et al., 2017). These groundwater supplies occur all along the lagoon (Fakir et al., 2019) and are predominantly linked to the extended karstic aquifer of the Coastal Sahel of Oualidia (Fakir et al., 2002; Kaid Rassou et al., 2005; Bouchaou et al., 2017). Its upper part (i.e., the most exploited for freshwater consumption) is composed of a 50 m thick Plio-Quaternary limestone-sandstone overlying a less permeable level of upper Hauterivian red clays. Below, the 30 m thick Dridrate limestone formation represents the lower aquifer which is less exploited but still provide the most abundant freshwater resources (Fakir et al., 2002; Kaid Rassou et al., 2005). Finally, the upper Valanginian marls constitute the substratum of the Dridrate aquifer and covers the Berriasian limestones, the upper Jurassic limestones rich in gypsum levels, and Triassic evaporites (Fakir et al., 2002; Fadili et al., 2015). According to Fakir et al. (2002), the dissolution of evaporites would be responsible for high Sr concentrations in local groundwater, reaching 2 to 2.5 times the OOW value.

2.2. Salses-Leucate Lagoon (South of France)

The Salses-Leucate lagoon formed during the Flandrian (i.e., 15 kyr BP; Arnaud and Raimbault, 1969; Clanzig, 1987). It corresponds to a shallow coastal basin separated from the Mediterranean Sea by a sandy barrier interrupted by three narrow and dispatched marine inlets (two of them are artificial ones) (Ladagnous and Le Bec, 1997; Fig. 1B). The lagoon is 14 km long and 5 km wide, with an average water depth of 1.7 m reaching 3.7 m in its deepest areas (Stieglitz et al., 2013). The region of Salses-Leucate is characterized by a dry season typical of the Mediterranean climate, with annual rainfalls of 588 mm.yr⁻¹ and annual

evaporation rates of 1.5 m.yr^{-1} (Ladagnous and LeBec, 1997). Basically, wind-driven currents control the hydrodynamic balance of the lagoon by provoking lagoon outflows and Mediterranean seawater inflows, both of them overprinted by moderate tidal influences (i.e., tidal range of 0.40 m; Ladagnous and le Bec, 1997). The lagoon hydrology is affected by freshwater inputs from two main karstic systems in its southwestern parts (i.e., the Font Dame and Font Estramar discharges) that are responsible for 98% of freshwater inputs into the lagoon, with fluxes of 8400 and $12500 \text{ m}^3.\text{h}^{-1}$ respectively (Ladagnous and Le Bec, 1997; Stieglitz et al., 2013). Altogether, these parameters produce spatial and seasonal salinity variations in the lagoon ranging from 20 to 30 (Bejannin et al., 2017). Finally, it is worth noting that the Font Estramar and Font Dame karstic resurgences belong to the well-studied Corbières karstic domain, which is composed of Jurassic and Cretaceous dolomites, limestones and marls covering Triassic evaporites, and constitutes one of the biggest karstic network from Europe (Ladouche and Dörfliger 2004; Aunay et al., 2003).

2.3. Banyuls-sur-Mer transect (South of France)

The Banyuls-sur-Mer (BSM) coast is located on the most eastern part of the Pyrenean reliefs (i.e., Massif des Albères) where the substratum lithology is dominated by metamorphic and crystalline continental rocks of Cambrian age (Fig. 1C; Got and Stanley, 1974). Influenced by a Mediterranean climate (with annual rainfalls of 575 mm.yr^{-1}), this open rocky coast displays no major freshwater input apart from the Baillaury river (mean flow rate of $0.2 \text{ m}^3.\text{s}^{-1}$) that can show very important freshwater discharges in rainy season (up to $165 \text{ m}^3.\text{s}^{-1}$ during floods). BSM is characterized by a low tidal range with an average of 0.40 m. From the BSM beach, a 25 km-long W-E transect was carried out at sea up to the Lacaze-Duthiers (LD) Canyon in order to collect surface and bottom seawater (i.e., up to 450 m water depth in the canyon). The LD canyon is one of the numerous canyons of the Gulf of Lion, with a strong bottom current and high-suspended sediment supplies from seasonal gravity flow

events (Heussner et al., 2006). The salinity and temperature of seawater is regularly measured by the Oceanological Observatory of Banyuls-sur-Mer in the framework of the SOMLIT program, both at SOLA (in the Banyuls Bay) and MOLA (offshore above the canyon) buoys. The surface seawater salinity varies between 34 and 38 whereas bottom seawater varies between 37 and 39. The salinity at 450 m depth fluctuates slightly around 38 (Durrieu de Madron et al., 2013).

2.4. The Tatakoto lagoon (French Polynesia, Pacific Ocean)

The Tatakoto lagoon is a semi-enclosed hemipelagic carbonate platform located in the eastern Tuamotu Archipelago in the Pacific Ocean (Fig. 1D). This archipelago spreads over 1600 km and is characterized by 77 atolls whose reef-barrier caps volcanic basement dated between 44 and 37.5 Myrs (Rougerie, 1994; Pirazzoli, 1998). The climate is tropical and dominated by a seasonal rainfall regime of 50 to 100 mm monthly from June to October and 100 to 200 mm monthly from November to May (Andréfouët et al., 2001). The Tatakoto atoll is about 12 km long and 3 km large, and the lagoon covers an area of $\sim 12 \text{ km}^2$ (Gilbert et al., 2006) with a maximal water depth measured at 18 m (C. Brahmi, personal communication). The atoll rim is closed in the northern part and semi-opened in the southern part. Water exchanges between the lagoon and the ocean occur through several shallow inlets located on the southern side and seawater mixing depends on tide, wave and wind regimes (Andréfouët et al., 2012; Van Wynsberge et al., 2017). The seawater exchanges between the atoll inner parts and ocean are weak owing to the low tidal range (with a maximum amplitude of 0.2 to 0.35 m). In the Tuamotu islands, water percolation through the reef porosity (i.e., 30 to 60%) is linked to erosion-dissolution and karstification processes (Rougerie, 1994). Note that intermediate oceanic seawaters flow through the porosity network of the barrier by endo-upwelling convection, leading to the formation of interstitial waters representing $\sim 50\%$ of the barrier volume (Rougerie, 1994). Thus, the renewal of the atoll seawater volume requires

several weeks up to several months depending on the morphology, the porosity of the barrier and the seasonal hydroclimatic conditions (Rougerie, 1994; Tartinville et al., 1997). Combined with evaporation rates of 0.5 to 1 m.yr⁻¹, all these processes impose lagoonal salinities fluctuating between 30 and 44 (Rougerie et al., 1984).

3. Material and Methods

3.1. Water and mollusc sampling

In order to check the spatial variability of seawater ⁸⁷Sr/⁸⁶Sr ratios in coastal domains, 38 water samples and 18 carbonate shells of living molluscs (i.e., bivalves and gastropods) were collected at the four studied sites (Fig. 1; Tables 1 and 2). When and where possible, we collected both the surface and bottom seawater together with molluscs for a given position.

In the field, the water samples were collected in 1L LDPE bottles previously cleaned with ultrapure 1N HCl, filtered *in situ* using 60 ml sterile plastic syringes with 0.2 µm Millipore filters (*in-situ* ultrafiltration was not possible in the field due to logistic constraints). All water samples are void of any microparticles usually found as suspended particle matter in the natural environment. *In-situ* filtration during water collection can significantly reduce microparticle-water interaction and therefore improve the characterization of the dissolved chemical pool (Cotte et al., 2015). They were stored at 4°C in a cold room prior to any sample preparation in a clean laboratory for chemical analyses. In the Oualidia and Salses-Leucate coastal lagoons, the water samples were collected (in April and June 2018, respectively) from 0 to 2 m water depth by diving from a chartered semi-rigid boat at various locations from landward parts affected by groundwater discharges to marine inlets and beaches facing the open marine realm (Fig. 1A,B). Bivalve shells from the Oualidia lagoon include *Crassostrea gigas*, *Venerupis decussata*, and *Solen marginatus*, whereas those from Salses-Leucate correspond to *Mytilus galloprovincialis*, *Crassostrea sp.*, and *Glycymeris glycymeris*. Note

that it was possible to collect directly the groundwaters from the Font-Dame and Font-Estramar resurgences at Salses-Leucate lagoon. However, the groundwater discharges of the Oualidia lagoon are mostly submerged, sparse and difficult to locate without *in-situ* chemical and salinity monitoring (Fakir et al., 2019).

In the Tatakoto lagoon, two water samples and four *Tridacna maxima* shells have been all collected at 2 m depth from two locations: one close to the southern oceanic inlets and the other one in the northern quiescent part of the inner lagoon (Fig. 1D).

Finally, a proximal-distal transect between the BSM beach and LD Canyon was carried out in May 2018 using the oceanographic research ship Néréis II (Station research vessel of Banyuls-sur-Mer, TGIR French Oceanographic Fleet; Fig. 1C), with a regular sampling of both surface and bottom seawater (down to 450 m below sea level; with *ex-situ* water filtration) as well as shells (encompassing unidentified bivalves fragments, *Mytilus galloprovincialis* and one gastropod *Turritella communis*) using a sediment grab.

3.2. Chemical composition of waters and shells

All the analytical steps have been performed at the Geosciences Environnement Toulouse laboratory (France). First, the collected water samples were prepared in a clean laboratory for chemical analyses including major (Mg, Ca, Na, K) and trace (Sr) element concentrations as well as the anion (Cl, SO₄, Br) concentrations. Anions were determined by anionic chromatography calibrated with an IAPSO seawater standard solution that was diluted at different proportion with MQ-H₂O to cover the entire range of anion concentrations. The IAPSO solution is a seawater standard solution provided by OSIL (UK) and certified for its salinity. The major and trace elements (Ca, Mg, Na, K, Sr) concentrations were measured using an Inductively Coupled Plasma optical emission spectrophotometer (ICP-OES), Horiba Jobin Yvon Ultima 2. We used the IAPSO standard solution to calibrate the instruments (Besson et al., 2014).

The shell samples were abraded, cleaned with Suprapur® acetic acid, and rinsed in Milli-Q water to remove external impurities and periostracum. Smaller bivalves and gastropods samples were entirely crushed with an agate mortar to get a powder, whereas only the inner parts of the umbo (recording the entire life span of the organism) were microdrilled for larger bivalve shells. For major element concentrations of molluscs, we dissolved 10 mg of sample using double-distilled 1 M HNO₃ on a hot plate at 70°C. After evaporation of the solution to dryness, it was dissolved in 2N HNO₃ and diluted 100 times with MQ-H₂O. The solution was then analyzed for Mg, Ca, and Sr concentrations using an ICP-OES. The dissolved elements are 1000 times more concentrated than their limit of detection (>10ppb). The ICP-OES instrument was calibrated using a matrix-matched synthetic standard. One of the calibration solutions was measured every 5 samples to check the instrumental drift during the course of the analyses. The measurements achieved a precision of 2.3% for Ca, 2.8% for Mg and 4.3% for Sr, in line with previous analytical precision on Ca-rich sample (Chavagnac et al., 2005).

3.3. Sr isotopic compositions

To determine the ⁸⁷Sr/⁸⁶Sr ratios, 1 ml of filtered water was transferred to a Savillex beaker prior to evaporation on a hot plate at 70 °C and the residue was dissolved in 0.5 ml of 2N HNO₃. For the shells, ~10 mg of powder was dissolved in a Savillex beaker with 2N HNO₃ on a hot plate at 70°C and centrifuged to exclude any residual fraction. Strontium was isolated from resulting solutions using Eichrom Sr-Spec column, a conventional elution protocol (Pin et al., 2014). The isolated Sr fraction was dissolved with 2μl of 0.5N H₃PO₄ solution of which 1μl was loaded on a tungsten filament together with 1μl of Tantalum activator. The Sr isotopic composition was measured using a Thermo Triton Plus thermal ionization mass spectrometer. The ⁸⁷Sr/⁸⁶Sr ratios were defined as the average of 150 measurements of ion intensities following the static multi-collection mode normalized to

$^{86}\text{Sr}/^{88}\text{Sr} = 0.1194$. During the measurement period, the standard NBS 987 gave $^{87}\text{Sr}/^{86}\text{Sr}$ ratios of 0.710280 ± 0.000003 (2SD, standard deviations, $n = 5$). Over the 2018 year, the measured NBS 987 isotopic compositions provided an external reproducibility of 0.710280 ± 0.000012 (2SD; $n = 26$). Regarding international seawater standards (IAPSO and NASS-6), they were processed in the clean room laboratory in the same manner as for our samples for Sr chemical isolation. The external $^{87}\text{Sr}/^{86}\text{Sr}$ reproducibilities are 0.709179 ± 0.000007 (2SD; $n = 7$) for IAPSO and 0.709180 ± 0.000014 (2SD; $n = 5$) for NASS-6, which agree very well with their certified values of 0.709179 ± 0.000005 and 0.709173 ± 0.000018 , respectively (Neymark et al., 2014).

For the bivalve shells, we analyzed at repeated times the Sr isotopic composition of the JCT-1 international standard (a giant clam *Tridacna gigas*) treated in the clean room as for our shell samples. The measurements provide an external reproducibility of 0.709176 ± 0.000015 (2SD; $n = 11$) for a certified value of 0.709150 ± 0.000050 (Ohno and Hirata, 2007). For comparison purposes between the $^{87}\text{Sr}/^{86}\text{Sr}$ ratios reported in this study and the literature data (tables 1 and 2), the $^{87}\text{Sr}/^{86}\text{Sr}$ ratios were corrected by adjusting the measured NBS 987 standard reference value to a certified value of 0.710250.

3.4. Geochemical and Sr isotopic database

To better depict potential influences of groundwater in the Oualidia and Salses-Leucate lagoons, we compiled a dataset of published major and trace elements concentrations (Ca, Mg, Na, K, SO_4 , Cl, Br and Sr) and $^{87}\text{Sr}/^{86}\text{Sr}$ ratios corresponding to groundwaters representative of Moroccan aquifers ($n = 112$) and the Corbières aquifer in France ($n = 141$) (see supplementary data). In order to analyze the geochemical patterns at a worldwide scale, we also compiled a dataset gathering 522 $^{87}\text{Sr}/^{86}\text{Sr}$ ratios and 571 Sr concentrations representative of OOW and shelf waters (SW) (see supplementary data). As for our samples,

all $^{87}\text{Sr}/^{86}\text{Sr}$ ratios reported in the literature were corrected by adjusting their respective NBS 987 standard reference value to a certified value of 0.710250.

4. Results

4.1. $^{87}\text{Sr}/^{86}\text{Sr}$ of waters and shells

The $^{87}\text{Sr}/^{86}\text{Sr}$ ratios of lagoon waters and shells are reported in Tables 1 and 2. First, at the Tatakoto lagoon, waters and shells exhibit $^{87}\text{Sr}/^{86}\text{Sr}$ ratios at 0.709165 - 0.709171 and 0.709164 – 0.709182, respectively, which are both indistinguishable from the average OOW value of 0.709172 (Figs. 1D and 2A). Similarly, seawater collected at different water depths along the BSM transect presents a slight dispersion ranging from 0.709166 to 0.709176, but still around the OOW value (Figs. 1C). The only sample deviating from this world value is BA9 collected in the Banyuls-sur-Mer beach: it presents a low salinity of 20 and a $^{87}\text{Sr}/^{86}\text{Sr}$ ratio of 0.709206 slightly more radiogenic than the OOW range (Fig. 2A). Molluscs from the BSM transect present Sr isotope compositions between 0.709164 and 0.709175, all identical to those of surrounding water (Fig. 2A).

In the Salses-Leucate lagoon, the seawater $^{87}\text{Sr}/^{86}\text{Sr}$ ratios ranging from 0.709155 and 0.709170 are typical of the OOW variability range. Contrastingly, three water samples (LEU 6, 7, 8) from the western part of the lagoon display values ranging from 0.708903 to 0.709132, that is below the OOW variability range. However, these values are trending towards the signatures of the Font Dame and Font Estramar discharges (LEU 10, 11) at 0.708618 and 0.708401, respectively (Fig. 1B). Again, these relatively low isotopic ratios occur along a salinity drop from 37.4 to 11.8 (Fig. 2A). In this context, the least radiogenic Sr isotope composition is measured for the bottom water sample (LEU 8) compared to the surface one (LEU 7). Mollusc shells sampled in this lagoon present $^{87}\text{Sr}/^{86}\text{Sr}$ ratios varying between 0.709125 and 0.709177, being either similar to or less radiogenic than the OOW value (Table

2; Fig. 2A). Finally, it is worth mentioning that our isotopic results are within the variability of those obtained for local seawater and groundwater sampled in 1998, 2002 and 2012 by Ladouche et al. (2000), Ladouche and Dörfliger (2004) and Petelet-Giraud et al. (2016).

At the Oualidia lagoon, both seawater and mollusc shells display highly variable $^{87}\text{Sr}/^{86}\text{Sr}$ ratios ranging from 0.708389 to 0.709168 and 0.708939 to 0.709179, respectively (Tables 1 and 2; Figs. 1A and 2A). Downstream, close to Atlantic seawater incursions by the inlets, the $^{87}\text{Sr}/^{86}\text{Sr}$ ratios of waters stay within the OOW variability range, while they are less and less radiogenic upstream between the OU12 and OU8 locations (Table 1, Figs. 1 and 2). As in Salses-Leucate and Banyuls bay, this isotopic shift is accompanied by a salinity decrease from 37.2 to 9.9 (Fig. 2A). However, the water sample OU6 deviates from this general tendency: although close to the northern dam, it records a $^{87}\text{Sr}/^{86}\text{Sr}$ ratio typical of OOW values (Fig. 1A). Finally, we note that most bivalve shells record $^{87}\text{Sr}/^{86}\text{Sr}$ ratios typical of OOW values but different of surrounding water values (Fig. 2A, Table 2). Only the O4 sample (i.e., an endobenthic *Solen marginatus*) fits the general $^{87}\text{Sr}/^{86}\text{Sr}$ decrease of lagoonal waters.

4.2. Geochemical composition of waters

All concentrations of anions and major and trace elements measured on the collected waters are reported in Table 1. In order to determine the origin of the waters influencing the $^{87}\text{Sr}/^{86}\text{Sr}$ of local seawater, only the most discriminating elements such as Sr, SO_4 , and Ca are used here, plotted as function of salinity, and compared to published values of regional groundwater aquifers (Fig. 2).

In the Pacific Tatakoto atoll, seawater has salinity and $^{87}\text{Sr}/^{86}\text{Sr}$ ratios typical of OOW while they display lower Sr contents ($\sim 73.5 \mu\text{mol}\cdot\text{l}^{-1}$ against $88 \mu\text{mol}\cdot\text{l}^{-1}$ for OOW; Millero et al. 2008). Slight enrichments in SO_4 ($30.8 \text{ mmol}\cdot\text{l}^{-1}$) and Ca ($10.3 \text{ mmol}\cdot\text{l}^{-1}$) are recorded but still within the OOW variability range. These geochemical characteristics also concern most

water samples from the Mediterranean BSM transect, whatever the water depth, with respective Sr, SO₄ and Ca concentrations of 72.2 – 74.5 μmol·l⁻¹, 30.9 – 32 mmol·l⁻¹, and 11.2 – 12.2 mmol·l⁻¹. The only exception is the beach sample BA9 which low salinity value of 26.4 is mirrored by low element concentrations compared to those of OOW (Table 1 and Fig. 2).

Euhaline waters from the inner parts of the Oualidia and Salses-Leucate lagoons are also characterized by similar depletions in Sr and slight enrichments in Ca and SO₄ when compared to the areas described above. However, the element concentrations evolve differently in Salses Leucate and Oualidia while the salinity and ⁸⁷Sr/⁸⁶Sr are decreasing landward. In Salses-Leucate, the Sr, SO₄ and Ca contents are dropping down to 17.2 μmol·l⁻¹, 3.8 mmol·l⁻¹ and 3.5 mmol·l⁻¹, respectively, close to the Font Dame and Font Estramar discharges. In agreement with previous analyses of Ladouche et al. (2000) and Ladouche and Dörfliger (2004), these low concentrations are similar to those prevailing at the scale of the regional aquifer and the covariations between salinity, ⁸⁷Sr/⁸⁶Sr ratio and these elemental concentrations are consistent with freshwater-seawater binary mixing. In Oualidia, the salinity and ⁸⁷Sr/⁸⁶Sr decrease while Sr and Ca concentrations remain relatively high and stable (i.e., ~73 μmol·l⁻¹ and ~11.5 mmol·l⁻¹, respectively), except in the salt marshes where values are much higher (i.e., 117 μmol·l⁻¹ and 20.5 mmol·l⁻¹, respectively). Contrastingly the SO₄ contents decrease with salinity but toward a brackish groundwater end-member with anomalously high SO₄ concentrations (~15 mmol·l⁻¹). Oualidia geochemical patterns are compatible with the high Sr, SO₄, and Ca contents recorded in some Moroccan groundwater aquifers, and especially those related to the dissolution of Mesozoic carbonate and gypsum levels (see Supplementary data).

394

395 **5. Discussion**

396 Studies with high precision $^{87}\text{Sr}/^{86}\text{Sr}$ ratio have confirmed that modern oligotrophic
397 oceanic waters (OOW) without terrestrial inputs have a quite homogeneous $^{87}\text{Sr}/^{86}\text{Sr}$ ratio of
398 0.709172 with a variability range of only ± 0.000023 at the global scale (Andersson et al.,
399 1992; Winter et al., 1997; Huang and You, 2007; Huang et al., 2011; Mokadem et al., 2015;
400 Pearce et al., 2015; Trezzi et al., 2017; El Meknassi et al., 2018). This homogeneity is yet
401 regularly challenged for shelf domains as more radiogenic or unradiogenic terrestrial Sr
402 supplies from rivers or SGD can introduce a dispersion to the measured $^{87}\text{Sr}/^{86}\text{Sr}$ of 6×10^{-3} or
403 more (El Meknassi et al., 2018) (Fig. 3A). Nevertheless, this estimate mainly concerns
404 estuaries, fjords, bays or epeiric seas supplied by major river systems for which data are
405 relatively abundant (e.g., Ingram and Sloan, 1992; Jørgensen and Banoeng-Yakubo, 2001;
406 Négrel et al., 2005; Jørgensen et al., 2008; Wang and You, 2013; Eissa et al., 2016; Casse et
407 al., 2019). In this context, new Sr isotope data from open shelves and coastal lagoons become
408 crucial to get a better view of processes at play in neritic domains, especially those locations
409 deprived of river and delta influences. These areas represent 40 – 50% of the world coasts
410 (Dürr et al., 2011).

411

412 *5.1. Seawater $^{87}\text{Sr}/^{86}\text{Sr}$ ratios in oceanic and open shelf domains*

413 With an average Sr concentration of $87.4 \mu\text{mol}\cdot\text{l}^{-1}$ (de Villiers 1999), oceanic inflows
414 are the main dissolved Sr source to shelf domains and hemipelagic carbonate platforms. If
415 these oceanic inflows remain constant through time and sufficiently mixed with coastal waters,
416 locally homogeneous seawater and shell $^{87}\text{Sr}/^{86}\text{Sr}$ ratios close to OOW value of 0.709172
417 would be expected, even in semi-enclosed areas. Far from any terrestrial influence, this is
418 clearly illustrated in the isolated Tatakoto atoll where Pacific seawater is the main dissolved

Sr source, conveyed to the shelf by endo-upwelling circulation through the reef porosity followed by surface currents (Rougerie, 1994). Rainwater infiltrations responsible for fossil reef karstification and possibly volcanic basement weathering are important in the Tuamotu archipelago (Guy et al., 1992; Waljeski, 2003). However, unradiogenic Sr supplied from local SGD appears too limited to modify the OOW $^{87}\text{Sr}/^{86}\text{Sr}$ ratio of studied waters and giant clams in this Pacific atoll (Table 1 and 2).

In the nearshore domain exemplified by the 25 km-long Mediterranean BSM transect, seawater and shells from surface down to ~450 mbsl display a homogeneous $^{87}\text{Sr}/^{86}\text{Sr}$ ratio with an average value at 0.709171 ± 0.000008 (2SD; n=12) indistinguishable from the OOW value (El Meknassi et al., 2018). In the absence of noticeable dissolved Sr inputs from rivers or SGD, this implies that the Sr inputs resulting from boundary-exchange processes acting at the sediment-water interface are not sufficient to modify the seawater $^{87}\text{Sr}/^{86}\text{Sr}$ ratio in these well-mixed open shelf conditions. This contrasts with estuaries or deltas where dissolved Sr released from suspended particulate dissolution may alter the $^{87}\text{Sr}/^{86}\text{Sr}$ of seawater in a few months (Jones et al., 2014; Jeandel and Oelkers, 2015). Moreover, the shell data from the BSM transect indicate that the Sr isotope composition of local seawater did not significantly change over life spans of 2 to 3 years. However, these results do not preclude caution in paleoenvironmental interpretation of shell $^{87}\text{Sr}/^{86}\text{Sr}$ ratios from the BSM coast and more generally nearshore contexts. This is because SGD influence may strongly vary in time and space along continental margins (Burnett et al., 2006), and especially in the Gulf of Lion where SGD are very important (Rodellas et al., 2015).

In the foreshore zone, additional factors can impact the seawater $^{87}\text{Sr}/^{86}\text{Sr}$ ratios. This is illustrated by the BA9 water sample collected on the BSM sandy beach, characterized by a more radiogenic value and a much lower salinity (i.e., 26.4) than the other samples. We propose that this more radiogenic Sr value can be related to three factors typical of intertidal

zones: 1) mixing with rainwater whose regional $^{87}\text{Sr}/^{86}\text{Sr}$ ratios range from 0.708993 to 0.709225 (Khaska et al., 2013), 2) sparse groundwater supplies whose Sr concentrations and radiogenic $^{87}\text{Sr}/^{86}\text{Sr}$ ratios mirror those from Quaternary, Pliocene, and Paleozoic aquifers (i.e., 0.708142 to 0.713782; Petelet et al., 1998; Petelet-Giraud et al., 2016), and 3) important dissolved Sr amounts released from suspended sandy particles continuously shaken in the surf zone (Kalnejais et al., 2010; Jeandel, 2016; Fabre et al., 2019) with particles $^{87}\text{Sr}/^{86}\text{Sr}$ ratios of 0.72232 – 0.72901 reflecting their metamorphic substratum (Brems et al., 2013). At broader scale, similar local processes can explain part of isotopic deviations reported in the rare water and shell data from open shelves (e.g., North Sea, Gulf of Guinea, South China Sea; Jørgensen and Banoeng-Yakubo, 2001; Jørgensen et al., 2008; Huang et al., 2011; El Meknassi et al., 2018) (Fig. 3). Moreover, marginal areas are transition zones where the oceanic mixing is not instantaneous and may take several years according to littoral currents, coastal physiography, and shelf width (Liu et al., 2019) (Fig. 3B). Terrestrial dissolved Sr sources, even remote, could slightly impact local seawater $^{87}\text{Sr}/^{86}\text{Sr}$ ratios through cumulative effects. Thus, we advocate to reject any water and/or shell sample from beach or intertidal zones to infer modern or past OOW $^{87}\text{Sr}/^{86}\text{Sr}$ ratios.

5.2. $^{87}\text{Sr}/^{86}\text{Sr}$ patterns in restricted coastal domains

Supplementing sparse literature data (e.g., Müller et al. 1990b; Beck et al. 2013; Shao et al. 2018), the seawater and shell results from the Oualidia and Salses-Leucate lagoons show clear evidence that restricted coastal domains, even without river influence, display very distinct $^{87}\text{Sr}/^{86}\text{Sr}$ ratios depending on the respective contribution of oceanic and SGD influxes (Fig. 1): 1) quite homogeneous OOW $^{87}\text{Sr}/^{86}\text{Sr}$ ratios except in close vicinity of SGD in Salses-Leucate; or 2) variable $^{87}\text{Sr}/^{86}\text{Sr}$ ratios ranging from OOW values at oceanic inlets to unradiogenic signals in the upstream parts of the Oualidia lagoon.

At broader scale, such Sr isotopic variabilities are also noticeable in epeiric seas. By compiling literature data and excluding the anomalous $^{87}\text{Sr}/^{86}\text{Sr}$ ratios (i.e., samples from beach or close to SGD) from Salses-Leucate, Banyuls-sur-Mer and Venice (Fig.4A), we observe that seawater $^{87}\text{Sr}/^{86}\text{Sr}$ ratios are typical of OOW values in western Mediterranean Sea (i.e., Spain, France, Italy), whereas those from eastern domains like the Bannock Basin, Aegean Sea, Marmara Sea and Black Sea decrease down to 0.70912 (this study; Müller et al., 1990a; Clauer et al., 2000; Peckmann et al., 2001; Major et al., 2006; Beck et al., 2013; Petelet-Giraud et al., 2016; Trezzi et al., 2017; Teichert et al., 2018). Highlighted here for the first time, these regional $^{87}\text{Sr}/^{86}\text{Sr}$ variations are consistent with the isotopic variability of Mediterranean water masses illustrated by the Nd isotopes (Tachikawa et al. 2004). Whether local or supra-regional, spatial Sr isotopic variability is insightful to decipher the respective influence of SGD and oceanic inputs on the Sr isotope budget of semi-enclosed areas.

5.2.1. SGD influences

With relatively high Sr concentrations (i.e., $2.9 \mu\text{mol}\cdot\text{l}^{-1}$) compared to river waters (i.e., 0.5 to $1.2 \mu\text{mol}\cdot\text{l}^{-1}$), SGDs represent an unradiogenic Sr source that can account for 13 - 30% of the global Sr ocean budget (Basu et al., 2001; Krabbenhöft et al., 2010; Beck et al., 2013). Depending on their geochemical and hydrodynamical characteristics related to the age and nature of weathered rocks but also oceanic intrusions, meteoric recharges, and water residence time in the aquifers (e.g., Négrel et al., 2003; Fadili et al., 2016, 2015; Santoni et al., 2016), their impact on the elemental and isotopic Sr budgets are, however, highly variable in coastal domains (e.g., Beck et al., 2013; Trezzi et al., 2017; Shao et al., 2018). This is illustrated by comparing the Salses-Leucate and Oualidia lagoons.

In the Salses-Leucate lagoon, the low salinities and the low Sr, SO_4 and Ca concentrations of Font Estramar and Font Dame discharges show that these groundwaters are

typical of meteoric freshwaters percolating through the local karstic aquifer (Fig. 2B,C,D). To better constrain the origin of the collected seawaters in the lagoon, we applied the isotopic mixing equation (Albarède, 1996) to geochemical data of regional end members presented in Table 3:

$$^{87}\text{Sr}/^{86}\text{Sr}_{(\text{mix})} = \left(\frac{^{87}\text{Sr}/^{86}\text{Sr}_{(\text{SW})} \times [\text{Sr}]_{(\text{SW})} \times \%q_{(\text{SW})}}{[\text{Sr}]_{(\text{mix})}} \right) + \left(\frac{^{87}\text{Sr}/^{86}\text{Sr}_{(\text{GW})} \times [\text{Sr}]_{(\text{GW})} \times \%q_{(\text{GW})}}{[\text{Sr}]_{(\text{mix})}} \right)$$

,where the mixed water $^{87}\text{Sr}/^{86}\text{Sr}_{(\text{mix})}$ ratio varies between the local seawater (SW) and groundwater (GW) end members of given Sr concentrations and $^{87}\text{Sr}/^{86}\text{Sr}$ ratios, using mixed water Sr concentrations $[\text{Sr}]_{(\text{mix})}$ calculated from cumulative 10% increments of GW to SW. The low $^{87}\text{Sr}/^{86}\text{Sr}$ ratios of Font Estramar and Font Dame discharges correspond to the lowest isotopic values of regional groundwaters and indicate a preferential dissolution of Jurassic and Cretaceous carbonates characterized by low $^{87}\text{Sr}/^{86}\text{Sr}$ ratios compared to the Pliocene and Quaternary silicates ones (Fig. 4A; Petelet et al., 1998; Ladouche et al. 2000; Aquilina et al., 2002; Ladouche and Dörfliger 2004; Khaska et al., 2013; Petelet-Giraud et al., 2016). Given the low Sr concentrations of Jurassic and Cretaceous GW endmembers (Table 3; Fig. 2B), our results suggest that the SGD contribution to the lagoon Sr budget is broadly less than 15% despite local SGD fluxes exceeding $5.55 \text{ m}^3.\text{s}^{-1}$ (Fig. 4B; Ladagnous and Le Bec, 1997; Stieglitz et al., 2013).

In Oualidia, the dissolved Sr supply of SGD with much lower estimated fluxes of $0.2 - 1.6 \text{ m}^3.\text{s}^{-1}$ (Hilmi et al., 2005; Fakir et al. 2019) markedly modifies the seawater $^{87}\text{Sr}/^{86}\text{Sr}$ ratios within the upstream parts of the lagoon (Figs. 1A). These induced modifications can be related to considerable unradiogenic Sr inputs while maintaining constant dissolved Sr concentrations (Fig. 2A,B). Indeed, groundwaters from the Coastal Sahel of Oualidia exhibit variable but generally high Sr and Ca concentrations reaching 2 to 2.5 times the OOW value as well as high SO_4 amounts (Fakir et al., 2002; Hilmi et al., 2005; Fig. 2B,C,D). Even if oceanic water intrusions are not excluded in the coastal aquifer, specific Ca and SO_4 excesses

indicate that the higher Sr contents would result from a preferential dissolution of Sr rich gypsum and celestite (SrSO_4) present in the Jurassic (and Cretaceous) limestones (Fakir et al., 2002; Hilmi et al., 2005; Kaid Rassou et al., 2005; Bouchaou et al., 2017). This hypothesis is in agreement with the unradiogenic $^{87}\text{Sr}/^{86}\text{Sr}$ ratio of lagoon waters (i.e., down to 0.708389) whose values are close to Jurassic aquifers of Morocco (Bouchaou et al., 2017; Vinson et al., 2013) (Fig. 4A). We estimate that groundwater fluxes dissolving Mesozoic sulphates spatially contribute from ~10 to 60 % to the lagoon Sr budget, the higher Sr concentrations being related to high evaporation rates in the salt marshes (Fig. 4A). This Sr supply markedly varied in a few years, as shown by the isotopic scatter between local seawater and shell data at a same location or shells sampled in 2006 (El Meknassi et al., 2018) and 2018 (this study) (Fig. 2A). In contrast, the low $^{87}\text{Sr}/^{86}\text{Sr}$ ratio recorded by one endobenthic *Solen marginatus* suggests that groundwater influence remained more constant in the interstitial waters at 80 cm sediment depth (i.e., the maximal burial depth of this species) than in the lagoon waters.

With Sr concentrations up to $150 \mu\text{mol}\cdot\text{l}^{-1}$ leading to local contributions of 60% to the Sr budget of lagoons, our results call to reconsider the importance of SGD in link to the dissolution of evaporitic deposits. In association with geothermal brines, their impact on the global ocean Sr budget still remains difficult to appraise but could be regionally important given the proximity of Messinian or Triassic evaporites such as those of Mediterranean margins (e.g., Stein et al., 2000). Considering their elevated Sr concentrations, it is also important to note that, contrarily to river-dominated contexts requiring considerable freshwater inputs to alter the coastal seawater $^{87}\text{Sr}/^{86}\text{Sr}$ ratio, SGD may quickly change this isotopic ratio in euhaline conditions. Indeed, most major world river systems produce measurable effects on seawater $^{87}\text{Sr}/^{86}\text{Sr}$ ratios when salinity drops below an average threshold of 12 (Bryant et al., 1995). Only ~15, 10 and 5 % of the rivers have significant effects at salinities above 20, 25 and 30, respectively. In contrast, significant $^{87}\text{Sr}/^{86}\text{Sr}$ shifts

occur at salinities close to 32–35 in the studied lagoons (Fig. 2A). From a paleoenvironmental point of view, these results call to be very careful in any paleosalinity deduction from coastal fossil $^{87}\text{Sr}/^{86}\text{Sr}$ data, especially since saline SGD are difficult to detect from biosedimentary facies or seismic data compared with freshwater SGD (Lecher and Mackey, 2018; Goff, 2019).

5.3. Influence of water mass restriction

From small lagoons to larger epeiric areas like Mediterranean and Baltic seas, oceanic mixing is essential to buffer regional SGD and river effects and maintain homogeneous seawater $^{87}\text{Sr}/^{86}\text{Sr}$ patterns typical of OOW. However, water mass restriction imposed by geographic barriers and water column stratification may be highly variable from one domain to another one. In lagoons, the local OOW renewal is more or less perennial and important depending on their leaky, choked or restricted geomorphology (Kjerfve and Magill, 1989; Umgiesser et al., 2014). Basically, restricted and leaky lagoons are parallel to the coast and present, respectively, few to numerous inlets that allow an efficient oceanic water turnover (e.g. every one to a few days) driven by tidal dynamics and/or wind forcing (Kjerfve and Magill, 1989; Umgiesser et al., 2014). These characteristics contribute therefore to homogenize seawater $^{87}\text{Sr}/^{86}\text{Sr}$ ratio close to the OOW one like in the Salses-Leucate or Venice lagoons (Beck et al. 2013) (Fig. 1). To the extreme, choked lagoons are characterized by only one or two oceanic inlets with a dominant wind forcing implying several days to several months for a total water renewal in the lagoon (Kjerfve and Magill, 1989; Umgiesser et al., 2014). This situation applies to the Oualidia lagoon, with the exception that tides are an important factor in the local hydrodynamics (Hilmi et al. 2017). Based on numerical modelling of tidal currents at Oualidia, the time necessary for full lagoon water renewal was estimated to be one or a few days in close vicinity of oceanic inlet increasing up to 15 to 30 days in the upstream channel and salt marshes, respectively (Hilmi et al., 2005, 2009, 2017).

As a result, the duality and rhythmicity between SGD discharges and seawater tidal influxes explain the $^{87}\text{Sr}/^{86}\text{Sr}$ gradient observed in the Oualidia lagoon from the oceanic inlet towards the interior of the lagoon.

In epeiric seas, similar water mass restriction processes appear relevant to explain the variability of seawater $^{87}\text{Sr}/^{86}\text{Sr}$ ratios. The Mediterranean basin is very interesting in this respect as SGD with elevated Sr concentrations ($5 - 12 \mu\text{mol}\cdot\text{l}^{-1}$) and low $^{87}\text{Sr}/^{86}\text{Sr}$ ratios (i.e., $0.7078 - 0.7080$) prevail all along the northern Mediterranean margin (Rodellas et al., 2015; Trezzi et al. 2017). However, only the eastern Mediterranean waters are significantly affected by these unradiogenic terrestrial Sr inputs (Fig. 3A). We propose that this spatial heterogeneity can be due to an efficient buffering of SGD in the western Mediterranean areas due to Atlantic OOW inflows from the strait of Gibraltar. Indeed, the renewal time of intermediate and deep waters is estimated to be 2.5 to 5 times faster in the western Mediterranean basin than it is in the eastern basin owing to the Sicily Strait (Tanhua et al., 2013).

By summarizing, we identify significant deviations from the OOW $^{87}\text{Sr}/^{86}\text{Sr}$ ratio in various marine contexts where the interplay between oceanic and terrestrial Sr inputs is a key parameter. This relative variability attests that, depending on their isolation, shelf domains may be regarded as dynamic and transitory Sr sub-reservoirs not always representative of the global ocean reservoir for which the modern Sr residence time is estimated around 2.5 Myr (Hodell et al., 1990). This spatial decoupling in the Sr budget was suggested by de Villiers (1999) for the upper ocean by estimating partial Sr residence times of only 5800–700,000 years in the upper 400 m of the water column due to a group of celestite (SrSO_4)-secreting radiolarians (i.e., Acantharia). In semi-enclosed coastal domains with transient dynamics like lagoons or large epeiric seas, we expect that the partial residence time (*sensu* Lin and Liu, 2019) could be in the same order of magnitude as water renewal time in marginal basins (i.e.,

one day to half a month for studied lagoons up to 30–130 years, 2–40 years, and 5–625 years in the Mediterranean, Baltic and Black Sea basins, respectively) (Lee et al., 2002; Stieglitz et al., 2017; Tanhua et al., 2013; Omstedt et al., 2014; Hilmi et al., 2017).

Finally, it worth noting that the Sr concentrations measured in the studied marine areas are relatively low (i.e., 60 – 70 $\mu\text{mol}\cdot\text{l}^{-1}$) compared with those of OOW (i.e., 80 – 90 $\mu\text{mol}\cdot\text{l}^{-1}$) (Fig. 2B). However, these results are in agreement with the large variability of coastal Sr concentrations (i.e., $\pm 20 \mu\text{mol}\cdot\text{l}^{-1}$) reported in worldwide coastal contexts (Fig. 5), sometimes with important annual fluctuations and local heterogeneities in euhaline waters (Ladouche et al., 2000; Brunskill et al., 2003; Elsdon and Gillanders, 2006). This suggests that the slightly non-conservative behaviour of Sr in seawater could be locally enhanced in some coastal and hemipelagic domains. Whether perennial or temporary, the cause of Sr depletions in euhaline waters – already reported the Salses-Leucate lagoon (Ladouche et al. 2000) but also sporadically observed along the Panama coast, in the Venice lagoon (Italy) or in the Gulf of Papua (Papua New Guinea) (Brunskill et al. 2003; Beck et al. 2013) - remains obscure. We hypothesize that, in some water mass restriction contexts, three factors could be involved and combined: 1) binding of Sr at the surface of sedimentary particles depending on grain size, iron and manganese oxides, and organic matter (Takada et al. 2014); 2) fast biological adsorption rates by specific organisms (i.e., see Bowen 1956, de Villiers 1999); or 3) influences of saline SGD (i.e., similar to superficial porewaters) slightly depleted in Sr and with isotopic ratios close to the one of seawater (e.g., Kastner et al. 1990).

Conclusion

In this study, we analyzed and compared the $^{87}\text{Sr}/^{86}\text{Sr}$ ratios and the major and trace element concentrations of seawaters and shells from marginal and hemipelagic contexts with different degrees of water mass restriction. Homogeneous $^{87}\text{Sr}/^{86}\text{Sr}$ ratios typical of OOW (i.e.,

0.709172 \pm 0.000023) are recorded in the Tatakoto atoll and along the BSM transect. This suggests that, in open shelf context without any river inputs, alternative Sr source like SGD or particulate dissolution are too limited and likely buffered by oceanic Sr inputs. This comforts the use of carbonate fossils from these domains to infer past OOW compositions. However, slight isotopic shifts may be observed in the foreshore area (e.g., BSM beach) that we interpret as resulting from rainwater mixing, local groundwater discharges or particle dissolution in the surf zone. Elevated coastal water retention times could also account for sporadic anomalous $^{87}\text{Sr}/^{86}\text{Sr}$ ratios in open shelves. In semi-enclosed domains, we report variable Sr isotope patterns between the studied karstic lagoons, with homogeneous seawater $^{87}\text{Sr}/^{86}\text{Sr}$ ratios typical of OOW (i.e., 0.709155 to 0.709170) in the Salses-Leucate lagoon (except close to groundwater discharges where the values drop to 0.708903) and an important $^{87}\text{Sr}/^{86}\text{Sr}$ gradient from OOW values close to the Atlantic inlet to less radiogenic values of 0.707957 in the upstream parts of the Oualidia lagoon. We relate these differences to two main factors. First, we note that, despite lower fluxes, the Oualidia lagoon is supplied by SGD with unradiogenic $^{87}\text{Sr}/^{86}\text{Sr}$ ratios and very high Sr concentrations (up to 150 $\mu\text{mol}\cdot\text{l}^{-1}$) linked to the dissolution of Mesozoic evaporites. These inputs lead to maximal contributions of 60% to the local Sr budget. The second parameter concerns the leaky, restricted or choked morphology of lagoons which controls the oceanic Sr inputs and thus buffers more or less any terrestrial Sr inputs through water mass homogenization. These two parameters appear also relevant to explain the $^{87}\text{Sr}/^{86}\text{Sr}$ gradient prevailing from west to east in the Mediterranean basin.

Acknowledgement

This study is a contribution of the MALACO project financed by the French national program LEFE/INSU. We thank the crew of the RV Nereis II and ‘Service at Sea’ from Banyuls

Oceanological Observatory (OOB) for their assistance in fieldwork as well as C. Destrigneville for analytical advices. We thank M. Böttcher for editorial handling and the four reviewers for their valuable remarks which considerably improved the manuscript.

Figure Captions

Fig. 1: Location and $^{87}\text{Sr}/^{86}\text{Sr}$ ratios of seawater and groundwater samples collected in the four studied sites: Oualidia lagoon (A), Salses-Leucate lagoon (B), Banyuls-sur-Mer (BSM) transect (C), Tatakoto atoll (D). Dashed lines indicate groundwater discharges.

Fig. 2: $^{87}\text{Sr}/^{86}\text{Sr}$, Sr, Ca, and SO_4 concentrations of waters as a function of salinity. (A) For a same sampling position with a given salinity, the $^{87}\text{Sr}/^{86}\text{Sr}$ ratios of living mollusc shells are compared to $^{87}\text{Sr}/^{86}\text{Sr}$ ratios of ambient seawater as well as oysters sampled in 2006 by El Meknassi et al. (2018) (see Table 2 for samples correspondence). Additional literature data from Salses-Leucate (i.e., water sampled in 1998, 2002 and 2012) are represented by squares with white contours (Ladouche et al. 2000; Ladouche and Dörfliger 2004; Petelet-Giraud et al. 2016). The isotopic range and the average elemental concentrations of OOW are from El Meknassi et al. (2018) and Millero et al., (2008), respectively. The salinity threshold defining significant influence of river water (RW) inputs on seawater $^{87}\text{Sr}/^{86}\text{Sr}$ ratios is from Bryant et al. (1995). Seawater and SGD values from the Oualidia and Salses-Leucates lagoons are compared to groundwater data available at the scale of Moroccan aquifers (Fakir et al., 2002; Kaid Rassou et al., 2005; Vinson et al. 2013; Fadili et al., 2015; Bouchaou et al., 2017) and the Corbières aquifer (southern France) (Petelet et al., 1998; Aquilina et al., 2002; Khaska et al., 2013; Petelet-Giraud et al., 2016). The analytical uncertainty bars are smaller than the width of symbols.

669

670 Fig. 3: (A) Worldwide distribution of published and new $^{87}\text{Sr}/^{86}\text{Sr}$ ratios for euhaline to
671 brackish shelf waters and oligotrophic oceanic waters (OOW). If locally variable, the
672 maximal and minimal $^{87}\text{Sr}/^{86}\text{Sr}$ ratios are represented by two colours. Box-and-whisker plot
673 corresponds to the OOW $^{87}\text{Sr}/^{86}\text{Sr}$ variability range published by El Meknassi et al. (2018).
674 Literature data from Müller et al. (1990a, 1990b), Andersson et al. (1992), Ingram and Sloan
675 (1992), Winter et al. (1997), Barker et al. (1998), Israelson and Buchardt (1999), Clauer et al.
676 (2000), Ladouche et al. (2000), Jørgensen and Banoeng-Yakubo (2001), Peckmann et al.
677 (2001), Wang et al. (2001), Négrel et al. (2005), Major et al. (2006), Huang and You (2007),
678 Sharma et al. (2017), Xu and Marcantonio (2017), Jørgensen et al. (2008), Martin and moore
679 (2008), Huang et al. (2011), Patra et al. (2012), Rahaman and Singh (2012), Beck et al. (2013),
680 Uddin et al. (2013), Wang and You (2013), Jones et al. (2014), Mokadem et al. (2015), Pearce
681 et al. (2015), Eissa et al. (2016), Petelet-Giraud et al. (2016), Trezzi et al. (2017), Shao et al.
682 (2018), Teichert et al. (2018), Casse et al. (2019), Danish et al. (2020).

683

684 Fig. 4: $^{87}\text{Sr}/^{86}\text{Sr}$ vs. $1/\text{Sr}$ diagram for the Salses-Leucate (A) and Oualidia (B) lagoon waters.
685 The data are compared to mixing trends between local seawater and different groundwaters
686 (GW) from Moroccan (A) and Corbières aquifers (B). End members data are presented in
687 Table 3. The mixing curves show the $^{87}\text{Sr}/^{86}\text{Sr}$ ratios for each 10 % increment. The analytical
688 uncertainty bars are smaller than the width of symbols.

689

690 Fig. 5: Sr concentration of shelf (SW) and oligotrophic oceanic (OOW) waters as a function
691 of salinity. The OOW data are from de Villiers (1999) and the SW data are compiled from
692 various sources (see supplementary data). The red and grey lines represent the linear
693 regression and the 95% confidence interval of Sr concentration values, respectively.

Table 1: $^{87}\text{Sr}/^{86}\text{Sr}$ and elemental concentrations of surface and bottom seawater from the studied sites.

Table 2: $^{87}\text{Sr}/^{86}\text{Sr}$ and elemental concentrations of studied shells.

Table 3: Average, minimal and maximal $^{87}\text{Sr}/^{86}\text{Sr}$ and Sr concentrations of seawater (SW) and groundwater (GW) end members used for mixing model of Fig. 4. GW data refer to waters percolating through different aquifers of the Corbières region (South France) and Morocco. As GW $^{87}\text{Sr}/^{86}\text{Sr}$ and Sr concentration data are missing or sparse, respectively, for the Coastal Sahel of Oualidia, we used GW data from Moroccan aquifers with host rocks of the same age and lithology (see supplementary data).

Bibliography

Albarède, F., 1996. Introduction to geochemical modeling. Cambridge University Press. 543pp.

Andersson, P.S., Wasserburg, G.J., Ingri, J., 1992. The sources and transport of Sr and Nd isotopes in the Baltic Sea. *Earth Planet. Sci. Lett.* 113, 459–472.
[https://doi.org/10.1016/0012-821X\(92\)90124-E](https://doi.org/10.1016/0012-821X(92)90124-E)

Andréfouët, S., Pagès, J., Tartinville, B., 2001. Water renewal time for classification of atoll lagoons in the Tuamotu Archipelago (French Polynesia). *Coral Reefs* 20, 399–408.
<https://doi.org/10.1007/s00338-001-0190-9>

Andréfouët, S., Ardhuin, F., Queffeuilou, P., Le Gendre, R., 2012. Island shadow effects and the wave climate of the Western Tuamotu Archipelago (French Polynesia) inferred from altimetry and numerical model data. *Mar. Pollut. Bull.* 65, 415–424.

719 <https://doi.org/10.1016/j.marpolbul.2012.05.042>

720 Aquilina, L., Ladouche, B., Doerfliger, N., Seidel, J.L., Bakalowicz, M., Dupuy, C., Le Strat,
721 P., 2002. Origin, evolution and residence time of saline thermal fluids (Balaruc springs,
722 southern France): Implications for fluid transfer across the continental shelf. *Chem. Geol.*
723 192, 1–21. [https://doi.org/10.1016/S0009-2541\(02\)00160-2](https://doi.org/10.1016/S0009-2541(02)00160-2)

724 Arnaud, P., Raimbault, R., 1969. The Salses-Leucate Pond. Its principal physicochemical
725 characteristics and their variations (in 1955-1956 and from 1960-1968). *Rev. Trav. Inst.*
726 *Peches. Marit.* 33(4), 335-443.

727 Aunay, B., Strat, P. le, Duvail, C., 2003. Méthode d'analyse géologique sur la karstification
728 des Corbières orientales et influence des évènements néogènes (tortonno-messiniens).
729 *Hydrol. Mediterr. semiarid Reg.* 278, 124–129.

730 Ballouche, A., Carruesco, C., 1986. Evolution holocène d'un écosystème lagunaire : la lagune
731 de Oualidia (Maroc atlantique). *Rev. géologie Dyn. géographie Phys.* 27, 113–118.

732 Bach, W., & Humphris, S. E., 1999. Relationship between the Sr and O isotope compositions
733 of hydrothermal fluids and the spreading and magma-supply rates at oceanic spreading
734 centers. *Geology*, 27(12), 1067-1070. [https://doi.org/10.1130/0091-](https://doi.org/10.1130/0091-7613(1999)027<1067:rbtsao>2.3.co;2)
735 [7613\(1999\)027<1067:rbtsao>2.3.co;2](https://doi.org/10.1130/0091-7613(1999)027<1067:rbtsao>2.3.co;2)

736 Barker, A.P., Newton, R.J., Bottrell, S.H. 1998. Processes affecting groundwater chemistry in
737 a zone of saline intrusion into an urban sandstone aquifer. *Applied Geochemistry*, 13,6,
738 735-749. [https://doi.org/10.1016/S0883-2927\(98\)00006-7](https://doi.org/10.1016/S0883-2927(98)00006-7)

739 Basu, A.R., Jacobsen, S.B., Poreda, R.J., Dowling, C.B., Aggarwal, P.K., 2001. Large
740 groundwater strontium flux to the oceans from the bengal basin and the marine strontium
741 isotope record. *Science* (5534). 293, 1470–1473.
742 <https://doi.org/10.1126/science.1060524>

743 Bataille, C.P., Willis, A., Yang, X., Liu, X., 2017. Continental igneous rock composition: A

major control of past global chemical weathering continental crust to seawater and exerts a direct control on several bio- surfaces have been invoked to explain some more specific features in screened database gath. Sci. Adv. 3, 1–16. <https://doi.org/10.1126/sciadv.1602183>

Beck, A.J., Charette, M.A., Cochran, J.K., Gonneea, M.E., Peucker-Ehrenbrink, B., 2013. Dissolved strontium in the subterranean estuary – Implications for the marine strontium isotope budget. *Geochim. Cosmochim. Acta* 117, 33–52. <https://doi.org/10.1016/J.GCA.2013.03.021>

Bejannin, S., van Beek, P., Stieglitz, T., Souhaut, M., Tamborski, J., 2017. Combining airborne thermal infrared images and radium isotopes to study submarine groundwater discharge along the French Mediterranean coastline. *J. Hydrol. Reg. Stud.* 13, 72–90. <https://doi.org/10.1016/j.ejrh.2017.08.001>

Bellefroid, E.J., Planavsky, N.J., Miller, N.R., Brand, U., Wang, C., 2018. Case studies on the utility of sequential carbonate leaching for radiogenic strontium isotope analysis. *Chem. Geol.* 497, 88–99. <https://doi.org/10.1016/j.chemgeo.2018.08.025>

Bouchaou, L., Warner, N.R., Tagma, T., Hssaisoune, M., Vengosh, A., 2017. The origin of geothermal waters in Morocco: Multiple isotope tracers for delineating sources of water-rock interactions. *Appl. Geochemistry* 84, 244–253. <https://doi.org/10.1016/j.apgeochem.2017.07.004>

Bowen, H.J.M. 1956. Strontium and barium in sea water and marine organisms. *J. Mar. Biol. Ass. U.K.*, 35, 451–460.

Brass, G., 1976. The variations of the marine $^{87}\text{Sr}/^{86}\text{Sr}$ ratio during Phanerozoic time: interpretation using a flux model. *Geochimica et Cosmochimica Acta* 40(7), 721–730. [https://doi.org/10.1016/0016-7037\(76\)90025-9](https://doi.org/10.1016/0016-7037(76)90025-9)

Brems, D., Ganio, M., Latruwe, K., Balcaen, L., Carremans, M., Gimeno, D., Silvestri, A.,

769 Vanhaecke, F., Muchez, P., Degryse, P., 2013. Isotopes on the beach, Part 1: Strontium
 770 isotope ratios as a provenance indicator for lime raw materials used in roman glass-
 771 making. *Archeometry*, 55(2), 214-234. doi: 10.1111/j.1475-4754.2012.00702.x
 772 Briard, J., Puceat, E., Vennin, E., Daeron, M., Chavagnac, V., Jaillet, R., Merle, D. And De
 773 Rafelis, M., 2020, Seawater paleotemperature and paleosalinity evolution in neritic
 774 environments of the Mediterranean margin: insights from isotope analysis of bivalve
 775 shells. *Paleogeo. Palaeoclim. Palaeoeco*, 543, DOI : 10.1016/J.palaeo.2019.109582
 776 Brunskill, G.J., Zagorskis, I., Pfitzner, J., 2003. Geochemical mass balance for lithium, boron,
 777 and strontium in the Gulf of Papua, new Guinea (Project TROPICS), *Geochimica et*
 778 *Cosmochimica Acta*, 67 (18), 3365-3383.
 779 Bryant, J.D., Jones, D.S., Mueller, A.A., 1995. Influence of freshwater flux on $^{87}\text{Sr}/^{86}\text{Sr}$
 780 chronostratigraphy in marginal environments and dating of vertebrate and invertebrate
 781 faunas. *Journal of Paleontology*, 69(1), 1-6.
 782 Burke, W.H., Denison, R.E., Hetherington, E.A., Koepnick, R.B., Nelson, H.F., Otto, J.B.,
 783 1982. Variation of seawater $^{87}\text{Sr}/^{86}\text{Sr}$ throughout Phanerozoic time. *Geology* 10, 516–519.
 784 [https://doi.org/10.1130/0091-7613\(1982\)10<516:VOSSTP>2.0.CO;2](https://doi.org/10.1130/0091-7613(1982)10<516:VOSSTP>2.0.CO;2)
 785 Burnett, W.C., Aggarwal, P.K., Aureli, A., Bokuniewicz, H., Cable, J.E., Charrette, M.A.,
 786 Kontar, E., Krupa, S., Kulkarni, K.M., Loveless, A., Moore, W.S., Oberdorfer, J.A.,
 787 Oliveira, J., Ozyurt, N., Povinec, P., Privitera, A.M.G., Rajar, R., Ramessur, R.T.,
 788 Scholten, J., Stieglitz, T., Taniguchi, M., Turner, J.V. 2006. Quantifying submarine
 789 groundwater discharge in the coastal zone via multiple methods. *Science of the Total*
 790 *Environement*, 367 (2-3), 498-543, doi: 10.1016/j.scitotenv.2006.05.009
 791 Casse, M., Montero-Serrano, J.C., St-Onge, G., Poirier, A., 2019. REE distribution and Nd
 792 isotope composition of estuarine waters and bulk sediment leachates tracing lithogenic
 793 inputs in eastern Canada. *Mar. Chem.* 211, 117-130.

794 <https://doi.org/10.1016/j.marchem.2019.03.012>

795 Chakrabarti, R., Mondal, S., Acharya, S.S., Lekha, J.S., Sengupta, D., 2018. Submarine
796 groundwater discharge derived strontium from the Bengal Basin traced in Bay of Bengal
797 water samples. *Sci. Rep.* 8, 1–10. <https://doi.org/10.1038/s41598-018-22299-5>

798 Chavagnac V., German C.R., Milton J. A., Palmer M.R., 2005. Source of REE in sediments
799 cores from the Rainbow vent site (36°14'N, MAR), *Chem. Geol.*, 216 (3-4), 329-352.
800 <https://doi.org/10.1016/j.chemgeo.2004.11.015>

801 Chavagnac, V., Leleu, T., Fontaine, F., Cannat, M., Ceuleneer, G., Castillo, A., 2018. Spatial
802 Variations in Vent Chemistry at the Lucky Strike Hydrothermal Field, Mid-Atlantic
803 Ridge (37°N): Updates for Subseafloor Flow Geometry From the Newly Discovered
804 Capelinhos Vent. *Geochemistry, Geophys. Geosystems* 19, 4444–4458.
805 <https://doi.org/10.1029/2018GC007765>

806 Clanzig, S., 1987. Inventaire des invertébrés d'une lagune méditerranéenne des côtes de
807 France, biocénoses et confinement: l'étang de Salses-Leucate (Roussillon). PhD Thesis,
808 Ecole Pratique des Hautes Etudes, Montpellier, France.

809 Clauer, N., Chaudhuri, S., Toulkeridis, T., Blanc, G., 2000. Fluctuations of Caspian Sea level:
810 Beyond climatic variations? *Geology* 28, 1015–1018. [https://doi.org/10.1130/0091-7613\(2000\)28<1015:FOCSLB>2.0.CO;2](https://doi.org/10.1130/0091-7613(2000)28<1015:FOCSLB>2.0.CO;2)

812 Cochran, J.K., Landman, N.H., Turekian, K.K., Michard, A., Schrag, D.P., 2003.
813 Paleooceanography of the Late Cretaceous (Maastrichtian) Western Interior Seaway of
814 North America: Evidence from Sr and O isotopes. *Palaeogeogr. Palaeoclimatol.*
815 *Palaeoecol.* 191, 45–64. [https://doi.org/10.1016/S0031-0182\(02\)00642-9](https://doi.org/10.1016/S0031-0182(02)00642-9)

816 Cotte, L., Waeles, M., Pernet-Coudrier, B., Sarradin, P.-M., Cathalot, C., Riso, R.D., 2015. A
817 comparison of in situ vs. ex situ filtration methods on the assessment of dissolved and
818 particulate metals at hydrothermal vents. *Deep-Sea Res.* 105, 186–194.

doi :10.1016/j.dsr.2015.09.005

- Danish, M., Tripathy G.R., Rahaman, W. 2020. Submarine groundwater discharge to a tropical costal lagoon (Chilika lagoon, India): An estimation using Sr isotopes. *Marine Chemistry*, 224, 103816, 1-13. <https://doi.org/10.1016/j.marchem.2020.103816>
- Davis, A.C., Bickle, M.J., Teagle, D.A.H., 2003. Imbalance in the oceanic strontium budget. *Earth Planet. Sci. Lett.* 211, 173–187. [https://doi.org/10.1016/S0012-821X\(03\)00191-2](https://doi.org/10.1016/S0012-821X(03)00191-2)
- de Villiers, S., 1999. Seawater strontium and Sr/Ca variability in the Atlantic and Pacific oceans. *Earth Planet. Sci. Lett.* 171, 623–634.
- DeVries, T., Primeau, F., 2011. Dynamically and Observationally Constrained Estimates of Water-Mass Distributions and Ages in the Global Ocean. *J. Phys. Oceanogr.* 41, 2381–2401. <https://doi.org/10.1175/jpo-d-10-05011.1>
- Dürr, H.H., Laruelle, G.G., van Kempen, C.M., Slomp, C.P., Meybeck, M., Middelkoop, H., 2011. Worldwide typology of nearshore coastal systems: Defining the estuarine filter of river inputs to the oceans. *Estuaries and Coasts* 34, 441-458. <https://doi.org/10.1007/s12237-011-9381-y>
- Durrieu De Madron, X., Houpert, L., Puig, P., Sanchez-Vidal, A., Testor, P., Bosse, A., Estournel, C., Somot, S., Bourrin, F., Bouin, M.N., Beauverger, M., Beguery, L., Calafat, A., Canals, M., Cassou, C., Coppola, L., Dausse, D., D’Ortenzio, F., Font, J., Heussner, S., Kunesch, S., Lefevre, D., Le Goff, H., Martín, J., Mortier, L., Palanques, A., Raimbault, P., 2013. Interaction of dense shelf water cascading and open-sea convection in the northwestern Mediterranean during winter 2012. *Geophys. Res. Lett.* 40, 1379–1385. <https://doi.org/10.1002/grl.50331>
- Eidvin, T., Vinzenz, C., Dybkjær, K., Skovbjerg, E., Piasecki, S., 2014. Discrepancy between Sr isotope and biostratigraphic datings of the upper middle and upper Miocene successions (Eastern North Sea). *Palaeogeogr. Palaeoclimatol. Palaeoecol.* 411, 267–280.

844 <https://doi.org/10.1016/j.palaeo.2014.07.005>

845 Eissa, M.A., Thomas, J.M., Pohll, G., Shouakar-Stash, O., Hershey, R.L., Dawoud, M., 2016.

846 Groundwater recharge and salinization in the arid coastal plain aquifer of the Wadi Watir

847 delta, Sinai, Egypt. *Appl. Geochemistry* 71, 48–62.

848 <https://doi.org/10.1016/j.apgeochem.2016.05.017>

849 Elsdon, T.S., Gillanders, B.M., 2006. Temporal variability in strontium, calcium, barium, and

850 manganese in estuaries: Implications for reconstructing environmental histories of fish

851 from chemicals in calcified structures. *Estuarine, Coastal and Shelf Science*, 66, 147-

852 156.

853 El Khalidi, K., Zourarah, B., Aajjane, A., 2011. Evolution récente de la morphologie de delta

854 de flot et son effet sur la dynamique hydro-sédimentaire de la lagune de Oualidia (Côte

855 Atlantique, Maroc): Approche par photographie aérienne. *Etudos do Quat. APEQ*, Braga,

856 7, 73–78.

857 El Meknassi, S. El, Dera, G., Cardone, T., Rafélis, M. De, Brahmi, C., Chavagnac, V., 2018.

858 Sr isotope ratios of modern carbonate shells : Good and bad news for chemostratigraphy

859 46 (11), 1003–1006. <https://doi.org/10.1130/G45380.1>

860 Fabre, S., Jeandel, C., Zambardi, T., Roustan, M., Almar, R., 2019. An overlooked silica

861 source of the modern oceans: Are sandy beaches the key? *Front. Earth Sci.*, 7, 231. doi:

862 10.3389/feart.2019.00231

863 Fadili, A., Mehdi, K., Riss, J., Najib, S., Makan, A., Boutayab, K., 2015. Evaluation of

864 groundwater mineralization processes and seawater intrusion extension in the coastal

865 aquifer of Oualidia, Morocco: hydrochemical and geophysical approach. *Arab. J. Geosci.*

866 8, 8567–8582. <https://doi.org/10.1007/s12517-015-1808-5>

867 Fadili, A., Najib, S., Mehdi, K., Riss, J., Makan, A., Boutayeb, K., Guessir, H., 2016.

868 Hydrochemical features and mineralization processes in coastal groundwater of Oualidia,

869 Morocco. J. African Earth Sci. 116, 233–247.
 870 <https://doi.org/10.1016/J.JAFREARSCI.2016.01.014>
 871 Fakir, Y., El Mernissi, M., Kreuser, T., Berjami, B., 2002. Natural tracer approach to
 872 characterize groundwater in the coastal Sahel of Oualidia (Morocco). Environ. Geol. 43,
 873 197–202. <https://doi.org/10.1007/s00254-002-0644-6>
 874 Fakir, Y., Claude, C., El Himer, H., 2019. Identifying groundwater discharge to an Atlantic
 875 coastal lagoon (Oualidia, Central Morocco) by means of salinity and radium mass
 876 balances. Environmental Earth Sciences. 78, 626. [https://doi.org/10.1007/s12665-019-](https://doi.org/10.1007/s12665-019-8637-x)
 877 8637-x
 878 Gilbert, A., Andréfouët, S., Yan, L., Remoissenet, G., 2006. The giant clam *Tridacna maxima*
 879 communities of three French Polynesia islands: comparison of their population sizes and
 880 structures at early stages of their exploitation. ICES J. Mar. Sci. 63, 1573–1589.
 881 <https://doi.org/10.1016/j.icesjms.2006.07.001>
 882 Goddérès, Y., Le Hir, G., Macouin, M., Donnadieu, Y., Hubert-Théou, L., Dera, G., Aretz, M.,
 883 Fluteau, F., Li, Z.X., Halverson, G.P., 2017. Paleogeographic forcing of the strontium
 884 isotopic cycle in the Neoproterozoic. Gondwana Res. 42, 151–162.
 885 <https://doi.org/10.1016/J.GR.2016.09.013>
 886 Goff, J.A., 2019. Modern and fossil pockmarks in the New England mud patch: Implications
 887 for submarine groundwater discharge on the middle shelf. Geophysical Research Letters,
 888 46 (21), <https://doi.org/10.1029/2019GL084881>
 889 Goldstein, S.J., Jacobsen, S.B., 1987. The Nd and Sr isotopic systematics of river-water
 890 dissolved material - Implications for the source of Nd and Sr in seawater. Chemical
 891 geology, 66(3-4), 245-272. [https://doi.org/10.1016/0168-9622\(87\)90045-5](https://doi.org/10.1016/0168-9622(87)90045-5)
 892 Got, H., Stanley, D.J., 1974. Sedimentation in two Catalanian canyons, northwestern
 893 Mediterranean. Mar. Geol. 16(5), M91-M100. <https://doi.org/10.1016/0025->

894 3227(74)90067-X

895 Guy, C., Schott, J., Destrigneville, C., Chiappini, R., 1992. Low-temperature alteration of
896 basalt by interstitial seawater, Mururoa, French Polynesia. *Geochim. Cosmochim. Acta*
897 56, 4169–4189. [https://doi.org/10.1016/0016-7037\(92\)90259-L](https://doi.org/10.1016/0016-7037(92)90259-L)

898 Heussner, S., Durrieu de Madron, X., Calafat, A., Canals, M., Carbonne, J., Delsaut, N.,
899 Saragoni, G., 2006. Spatial and temporal variability of downcore particle fluxes on a
900 continental slope: Lessons from an 8-yr experiment in the Gulf of Lions (NW
901 Mediterranean). *Mar. Geol.* 234, 63–92.

902 Hilmi, K., Koutitonsky, V.G., Orbi, A., Lakhdar, J.I., Chagdali, M., 2005. Oualidia lagoon,
903 Morocco: an estuary without a river. *African J. Aquat. Sci.* 30, 1–10.
904 <https://doi.org/10.2989/16085910509503828>

905 Hilmi, K., Orbi, A., Lakhdar Idrissi, J., 2009. Hydrodynamisme de la lagune de Oualidia
906 (Maroc) durant l ’été et l ’automne 2005. *Bull. l’Institut Sci. Rabat, Sect. Sci. la Terre*,
907 31, 29–34.

908 Hilmi, K., Makaoui, A., Ettahiri, O., Idrissi, M., Larissi, J., Abdellaoui, B., El Ouehabi, Z.,
909 Obri, A., 2017. Fonctionnement Hydrodynamique De La Lagune De Oualidia (Maroc)
910 Avant L’Amenagement De La Souille. *Int. J. Adv. Res.* 5, 2015–2027.
911 <https://doi.org/10.21474/ijar01/4937>

912 Hodell, D.A., Mead, G.A., Mueller, P.A., 1990. Variation in the strontium isotopic
913 composition of seawater (8 Ma to present) : Implications for chemical weathering rates
914 and dissolved fluxes to the oceans. *Chem. Geol. Isot. Geosci. Sect.* 80, 291–307.
915 [https://doi.org/10.1016/0168-9622\(90\)90011-Z](https://doi.org/10.1016/0168-9622(90)90011-Z)

916 Huang, K.F., You, C.F., 2007. Tracing freshwater plume migration in the estuary after a
917 typhoon event using Sr isotopic ratios. *Geophys. Res. Lett.* 34, 1–5.
918 <https://doi.org/10.1029/2006GL028253>

919 Huang, K.-F., You, C.-F., Chung, C.-H., Lin, I.-T., 2011. Nonhomogeneous seawater Sr
 920 isotopic composition in the coastal oceans: A novel tool for tracing water masses and
 921 submarine groundwater discharge. *Geochemistry, Geophys. Geosystems* 12, 1–14.
 922 <https://doi.org/10.1029/2010GC003372>

923 Ingram, B.L., Sloan, D., 1992. Strontium isotopic composition of estuarine sediments as
 924 paleosalinity-paleoclimate indicator. *Science* (5040). 255, 68–72. [https://doi:](https://doi.org/10.1126/science.255.5040.68)
 925 [10.1126/science.255.5040.68](https://doi.org/10.1126/science.255.5040.68)

926 Israelson, C., Buchardt, B., 1999. Strontium and oxygen isotopic composition of East
 927 Greenland rivers and surface waters: Implication for palaeoenvironmental interpretation.
 928 *Palaeogeogr. Palaeoclimatol. Palaeoecol.* 153, 93–104. [https://doi.org/10.1016/S0031-](https://doi.org/10.1016/S0031-0182(99)00068-1)
 929 [0182\(99\)00068-1](https://doi.org/10.1016/S0031-0182(99)00068-1)

930 Jeandel, C., 2016. Overview of the mechanisms that could explain the “Boundary Exchange”
 931 at the land-ocean contact. *Philos. Trans. R. Soc. A Math. Phys. Eng. Sci.* 374, 1–13.
 932 <https://doi.org/10.1098/rsta.2015.0287>

933 Jeandel, C., Oelkers, E.H., 2015. The influence of terrigenous particulate material
 934 dissolution on ocean chemistry and global element cycles. *Chem. Geol.* 395, 50–66.
 935 <https://doi.org/10.1016/j.chemgeo.2014.12.001>

936 Jones, M.T., Gislason, S.R., Burton, K.W., Pearce, C.R., Mavromatis, V., Pogge von
 937 Strandmann, P.A.E., Oelkers, E.H., 2014. Quantifying the impact of riverine particulate
 938 dissolution in seawater on ocean chemistry. *Earth Planet. Sci. Lett.* 395, 91–100.
 939 <https://doi.org/10.1016/j.epsl.2014.03.039>

940 Jørgensen, N.O., Andersen, M.S., Engesgaard, P., 2008. Investigation of a dynamic seawater
 941 intrusion event using strontium isotopes ($^{87}\text{Sr}/^{86}\text{Sr}$). *J. Hydrol.* 348, 257–269.
 942 <https://doi.org/10.1016/j.jhydrol.2007.10.001>

943 Jørgensen, N.O., Banoeng-Yakubo, B.K., 2001. Environmental isotopes (^{18}O , ^2H , and

944 $^{87}\text{Sr}/^{86}\text{Sr}$) as a tool in groundwater investigations in the Keta Basin, Ghana. *Hydrogeol. J.*
 945 9, 190–201. <https://doi.org/10.1007/s100400000122>
 946 Kaid Rassou, K., Fakir, Y., Bahir, M., Zouari, K., Marah, M., Monteiro, J.P., 2005. Apport
 947 des analyses isotopiques à la compréhension du fonctionnement des aquifères cotiers du
 948 bassin hydrologiques de la lagune d'Oualidia (Ocean Atlantique marocain).
 949 *Comuniceções Geol.*, 92, 129-142.
 950 Kalnejais, L.H., Martin, W.R., Bothner, M.H., 2010. The release of dissolved nutrients and
 951 metals from coastal sediments due to resuspension. *Mar. Chem.* 121, 224–235.
 952 <https://doi.org/10.1016/j.marchem.2010.05.002>
 953 Kastner, M., Elderfield, H., Martin, J.B., Suess, E., Kvenvolden, K.A., Garrison, R.E., 1990.
 954 Diagenesis and interstitial-water chemistry at the peruvian continental margin - Major
 955 constituents and strontium isotopes. *Proceedings of the Ocean Drilling Program,*
 956 *Scientific Results*, 112, 413-440.
 957 Khaska, M., Le Gal La Salle, C., Lancelot, J., ASTER, T., Mohamad, A., Verdoux, P., Noret,
 958 A., Simler, R., 2013. Origin of groundwater salinity (current seawater vs. saline deep
 959 water) in a coastal karst aquifer based on Sr and Cl isotopes. Case study of the La Clape
 960 massif (southern France). *Appl. Geochemistry* 37, 212–227.
 961 <https://doi.org/10.1016/j.apgeochem.2013.07.006>
 962 Kjerfve, B., Magill, K., 1989. Geographic and hydrodynamic characteristics of shallow
 963 coastal lagoons. *Mar. Geol.* 88, 187–199. [https://doi.org/10.1016/0025-3227\(89\)90097-2](https://doi.org/10.1016/0025-3227(89)90097-2)
 964 Krabbenhöft, A., Eisenhauer, A., Böhm, F., Vollstaedt, H., Fietzke, J., Liebetrau, V.,
 965 Augustin, N., Peucker-Ehrenbrink, B., Müller, M.N., Horn, C., Hansen, B.T., Nolte, N.,
 966 Wallmann, K., 2010. Constraining the marine strontium budget with natural strontium
 967 isotope fractionations ($^{87}\text{Sr}/^{86}\text{Sr}^*$, $\delta^{88}/^{86}\text{Sr}$) of carbonates, hydrothermal solutions and
 968 river waters. *Geochim. Cosmochim. Acta* 74, 4097–4109.

969 <https://doi.org/10.1016/j.gca.2010.04.009>

970 Ladagnous, H., Le Bec, C., 1997. La lagune de Salses-Leucate: I- Analyse bibliographique.
 971 Direction de l'environnement et de l'aménagement du littoral. R.INT.DEL/97.02/SETE.
 972 <https://archimer.ifremer.fr/doc/00073/18422/>

973 Ladouche, B., Le Bec, C., Aquilina, L., Bakalowicz, M., Souchu, P., Doerfliger, N., Anus, S.
 974 (2000) Recherche de l'origine de la contamination bactériologique de l'étang de Salses-
 975 Leucate. Rap. BRGM/RP-50003-FR, 64p

976 Ladouche, B., Dörfliger, N., 2004. Evaluation des ressources en eau des Corbières. Phase I -
 977 Synthèse de la caractérisation des systèmes karstiques des Corbières orientales. Rapport
 978 final. Volume 2 - caractérisation géologique et hydrogéologique du système karstique du
 979 "synclinal du bas-Agly". BRGM/RP-52919-FR, 196p.

980 Lecher, A.L., Mackey, K.R.M. 2018. Synthesizing the effects of submarine groundwater
 981 discharge on marine biota. *Hydrology*, 5, 60, doi:10.3390/hydrology5040060

982 Lee, B.S., Bullister, J.L., Murray, J.W., Sonnerup, R.E., 2002. Anthropogenic
 983 chlorofluorocarbons in the Black Sea and the Sea of Marmara. *Deep. Res. Part I*
 984 *Oceanogr. Res. Pap.* 49, 895–913. [https://doi.org/10.1016/S0967-0637\(02\)00005-5](https://doi.org/10.1016/S0967-0637(02)00005-5)

985 Li, Y-H., 1982. A brief discussion on the mean oceanic residence time of elements. *Geochim.*
 986 *Cosmochim. Acta* 46, 2671–2675.

987 Lin, L., Liu, Z., 2019. Partial residence times: determining residence time compositions in
 988 different subregions. *Ocean Dynamics*, 69, 1023-1036.

989 Liu, X., Dunne, J.P., Stock, C.A., Harrison, M.J., Adcroft, A., Resplandy, L., 2019.
 990 Simulating water residence time in the coastal ocean: A global perspective. *Geophysical*
 991 *Research Letters*, 46, 13,910–13,919. <https://doi.org/10.1029/2019GL085097>

992 Major, C.O., Goldstein, S.L., Ryan, W.B.F., Lericolais, G., Piotrowski, A.M., Hajdas, I., 2006.
 993 The co-evolution of Black Sea level and composition through the last deglaciation and its

994 paleoclimatic significance. *Quat. Sci. Rev.* 25, 2031–2047.
 995 <https://doi.org/10.1016/j.quascirev.2006.01.032>
 996 Marcano, M.C., Frank, T.D., Mukasa, S.B., Lohmann, K.C., Taviani, M., 2015. Diagenetic
 997 incorporation of Sr into aragonitic bivalve shells: implications for chronostratigraphic
 998 and palaeoenvironmental interpretations. *Depos. Rec.* 1, 38–52.
 999 <https://doi.org/10.1002/dep2.3>
 1000 Martin, J.B., Moore, P.J. 2008. Sr concentrations and isotope ratios as tracers of ground-water
 1001 circulation in carbonate platforms: Examples from San Salvador and Long Island,
 1002 Bahamas. *Chemical Geology*, 249, 52–65. [https://doi.org/](https://doi.org/10.1016/j.chemgeo.2007.11.009)
 1003 [10.1016/j.chemgeo.2007.11.009](https://doi.org/10.1016/j.chemgeo.2007.11.009)
 1004 Martin, E.E., Scher, H.D., 2004. Preservation of seawater Sr and Nd isotopes in fossil fish
 1005 teeth: bad news and good news. *Earth Planet. Sci. Lett.* 220, 25–39.
 1006 [https://doi.org/10.1016/S0012-821X\(04\)00030-5](https://doi.org/10.1016/S0012-821X(04)00030-5)
 1007 McArthur, J.M., 1994. Recent trends in strontium isotope stratigraphy. *Terra Nov.* 6, 331–358.
 1008 <https://doi.org/10.1111/j.1365-3121.1994.tb00507.x>
 1009 McArthur, J.M., Howarth, R.J., Shields, G.A., 2012. Strontium Isotope Stratigraphy, in: *The*
 1010 *Geologic Time Scale*. Elsevier, pp. 127–144. [https://doi.org/10.1016/B978-0-444-59425-](https://doi.org/10.1016/B978-0-444-59425-9.00007-X)
 1011 [9.00007-X](https://doi.org/10.1016/B978-0-444-59425-9.00007-X)
 1012 Millero, F.J., Feistel, R., Wright, D.G., McDougall, T.J., 2008. The composition of Standard
 1013 Seawater and the definition of the Reference-Composition Salinity Scale. *Deep Sea Res.*
 1014 *Part I Oceanogr. Res. Pap.* 55, 50–72. <https://doi.org/10.1016/J.DSR.2007.10.001>
 1015 Mokadem, F., Parkinson, I.J., Hathorne, E.C., Anand, P., Allen, J.T., Burton, K.W., 2015.
 1016 High-precision radiogenic strontium isotope measurements of the modern and glacial
 1017 ocean: Limits on glacial–interglacial variations in continental weathering. *Earth Planet.*
 1018 *Sci. Lett.* 415, 111–120. <https://doi.org/10.1016/J.EPSL.2015.01.036>

1019 Müller, D.W., Mueller, P.A., McKenzie, J.A., 1990a. Strontium Isotopic Ratios as Fluid
 1020 Tracers in Messinian Evaporites of the Tyrrhenian Sea (Western Mediterranean Sea).
 1021 Proc. Ocean Drill. Program, 107 Sci. Results 107, 603–614.
 1022 <https://doi.org/10.2973/odp.proc.sr.107.194.1990>
 1023 Müller, D.W., McKenzie, J.A., Mueller, P.A., 1990b. Abu Dhabi sabkha, Persian Gulf,
 1024 revisited: Application of strontium isotopes to test an early dolomitization model.
 1025 Geology 18, 618–621. [https://doi.org/10.1130/0091-](https://doi.org/10.1130/0091-7613(1990)018<0618:ADSPGR>2.3.CO;2)
 1026 [7613\(1990\)018<0618:ADSPGR>2.3.CO;2](https://doi.org/10.1130/0091-7613(1990)018<0618:ADSPGR>2.3.CO;2)
 1027 Négrel, P., Casanova, J., Blomqvist, R., Kaija, J., Frape, S., 2003. Strontium isotopic
 1028 characterization of the Palmottu hydrosystem (Finland): Water-rock interaction and
 1029 geochemistry of groundwaters. Geofluids 3, 161–175. [https://doi.org/10.1046/j.1468-](https://doi.org/10.1046/j.1468-8123.2003.00056.x)
 1030 [8123.2003.00056.x](https://doi.org/10.1046/j.1468-8123.2003.00056.x)
 1031 Négrel, P., Casanova, J., Blomqvist, R., 2005. $^{87}\text{Sr}/^{86}\text{Sr}$ of brines from the Fennoscandian
 1032 Shield: a synthesis of groundwater isotopic data from the Baltic Sea region. Can. J. Earth
 1033 Sci. 42, 273–285. <https://doi.org/10.1139/e04-103>
 1034 Neymark, L.A., Premo, W.R., Mel’Nikov, N.N., and Emsbo, P., 2014, Precise determination
 1035 of $\delta^{88}\text{Sr}$ in rocks, minerals, and waters by double-spike TIMS: A powerful tool in the
 1036 study of geological, hydrological and biological processes: Journal of Analytical Atomic
 1037 Spectrometry, v. 29, p. 65–75, [https://doi: 10.1039/c3ja50310k](https://doi.org/10.1039/c3ja50310k).
 1038 Nieto, L.M., Ruiz-Ortiz, P.A., Rey, J., Benito, M.I., 2008. Strontium-isotope stratigraphy as a
 1039 constraint on the age of condensed levels: examples from the Jurassic of the Subbetic
 1040 Zone (southern Spain). Sedimentology, 55, 1-28. [https://doi: 10.1111/j.1365-](https://doi.org/10.1111/j.1365-3091.2007.00891.x)
 1041 [3091.2007.00891.x](https://doi.org/10.1111/j.1365-3091.2007.00891.x)
 1042 Omstedt, A., Elken, J., Lehmann, A., Leppäranta, M., Meier, H.E.M., Myrberg, K.,
 1043 Rutgersson, A., 2014. Progress in physical oceanography of the Baltic Sea during the

1044 2003-2014 period. Progress in Oceanography, 128, 139-171.
 1045 <https://doi.org/10.1016/j.pocean.2014.08.010>
 1046 Ohno T., Hirata T., 2007. Simultaneous determination of mass-dependent isotopic
 1047 fractionation and radiogenic isotope variation of strontium in geochemical samples by
 1048 multiple collector-ICP-mass spectrometry. Analytical Science, 23, 1275–1280.
 1049 <https://doi.org/10.2116/analsci.23.1275>
 1050 Palmer, M.R., Edmond, J.M., 1989. The strontium isotope budget of the modern ocean. Earth
 1051 Planet. Sci. Lett. 92, 11–26. [https://doi.org/10.1016/0012-821X\(89\)90017-4](https://doi.org/10.1016/0012-821X(89)90017-4)
 1052 Palmer, M., Edmond, J., 1992. Controls over the strontium isotope composition of river water.
 1053 Geochim. Cosmochim. Acta 56, 2099–2111. [https://doi.org/10.1016/0016-](https://doi.org/10.1016/0016-7037(92)90332-D)
 1054 [7037\(92\)90332-D](https://doi.org/10.1016/0016-7037(92)90332-D)
 1055 Patra, S., Liu, C.Q., Wang, F.S., Li, S.L., Wang, B.L. 2012. Behaviour of major and minor
 1056 elements in a temperate river estuary to the coastal area. International Journal of
 1057 Environmental Science and Technology, 9(4), 655-660. [https://doi.org/10.1007/s13762-](https://doi.org/10.1007/s13762-012-0097-8)
 1058 [012-0097-8](https://doi.org/10.1007/s13762-012-0097-8)
 1059 Pearce, C.R., Parkinson, I.J., Gaillardet, J., Charlier, B.L.A., Mokadem, F., Burton, K.W.,
 1060 2015. Reassessing the stable ($\delta^{88/86}\text{Sr}$) and radiogenic ($^{87}\text{Sr}/^{86}\text{Sr}$) strontium isotopic
 1061 composition of marine inputs. Geochim. Cosmochim. Acta 157, 125–146.
 1062 <https://doi.org/10.1016/J.GCA.2015.02.029>
 1063 Peckmann, J., Reimer, A., Luth, U., Luth, C., Hansen, B.T., Heinicke, C., Hoefs, J., Reitner, J.,
 1064 2001. Methane-derived carbonates and authigenic pyrite from the northwestern Black
 1065 Sea. Mar. Geol. 177, 129–150. [https://doi.org/10.1016/S0025-3227\(01\)00128-1](https://doi.org/10.1016/S0025-3227(01)00128-1)
 1066 Petelet, E., Luck, J.-M., Ben Othman, D., Négrel, P., Aquilina, L., Brgm, F., 1998.
 1067 Geochemistry and Water Dynamics of a Medium-Sized Watershed: the Herault,
 1068 Southern France. Chem. Geol. 150, 63–83. <https://doi.org/10.1016/S0009->

1069 2541(98)00053-9

1070 Petelet-Giraud, E., Négrel, P., Aunay, B., Ladouche, B., Bailly-Comte, V., Guerrot, C.,
 1071 Flehoc, C., Pezard, P., Lofi, J., Dörfliger, N., 2016. Coastal groundwater salinization:
 1072 Focus on the vertical variability in a multi-layered aquifer through a multi-isotope
 1073 fingerprinting (Roussillon Basin, France). *Sci. Total Environ.* 566–567, 398–415.
 1074 <https://doi.org/10.1016/j.scitotenv.2016.05.016>

1075 Peterman, Z.E., Hedge, C.E., Tourtelot, H.A., 1970. Isotopic composition of strontium in sea
 1076 water throughout Phanerozoic time. *Geochim. Cosmochim. Acta* 34, 105–120.
 1077 [https://doi.org/10.1016/0016-7037\(70\)90154-7](https://doi.org/10.1016/0016-7037(70)90154-7)

1078 Peucker-Ehrenbrink, B., Miller, M.W., Arsouze, T., Jeandel, C., 2010. Continental bedrock
 1079 and riverine fluxes of strontium and neodymium isotopes to the oceans. *Geochemistry,*
 1080 *Geophys. Geosystems* 11, 1–22. <https://doi.org/10.1029/2009GC002869>

1081 Peucker-Ehrenbrink, B., Fiske, G.J., 2019. A continental perspective of the seawater
 1082 $^{87}\text{Sr}/^{86}\text{Sr}$ record: A review. *Chem. Geol.* 510, 140–165.
 1083 <https://doi.org/10.1016/J.CHEMGEO.2019.01.017>

1084 Pin C., Gannounb A., Dupont A., 2014. Rapid, simultaneous separation of Sr, Pb, and Nd by
 1085 extraction chromatography prior to isotope ratios determination by TIMS and MC-ICP-
 1086 MS. *Journal Analytical Atomic Spectrometry*, 29, 1858–1870. [https://doi:](https://doi.org/10.1039/C4JA00169A)
 1087 [10.1039/C4JA00169A](https://doi.org/10.1039/C4JA00169A)

1088 Pirazzoli, P.A., 1998. Sur la vitesse des variations du niveau de la mer, in: *Annales de*
 1089 *Géographie*, 107 (600), 220–232.

1090 Reeder, S.W., Hitchon, B., Levinson, A.A., 1972. Hydrogeochemistry of the surface waters of
 1091 the Mackenzie River drainage basin, Canada - I. Factor controlling inorganic
 1092 composition. *Geochimica et Cosmochimica Acta*, 36(8), 825–865.
 1093 [https://doi.org/10.1016/0016-7037\(72\)90053-1](https://doi.org/10.1016/0016-7037(72)90053-1)

1094 Rodellas, V., Garcia-Orellana, J., Masqué, P., Feldman, M., Weinstein, Y., 2015. Submarine
 1095 groundwater discharge as a major source of nutrients to the Mediterranean Sea. *Proc.*
 1096 *Natl. Acad. Sci.* 112, 3926–3930. <https://doi.org/10.1073/pnas.1419049112>
 1097 Rougerie, F., Ricard, M., Mazaury, E., Des, D., Iagonalres, E., 1984. Dynamique et échanges
 1098 lagon-océan modèle de circulation interne à travers le socle corallien. Report CEA-R-
 1099 5236.
 1100 Rougerie, F., 1995. Nature et fonctionnement des atolls des Tuamotu (Polynésie Française).
 1101 *Oceanol. Acta* 18, 61–78.
 1102 Santoni, S., Huneau, F., Garel, E., Aquilina, L., Vergnaud-Ayraud, V., Labasque, T., Celle-
 1103 Jeanton, H., 2016. Strontium isotopes as tracers of water-rocks interactions, mixing
 1104 processes and residence time indicator of groundwater within the granite-carbonate
 1105 coastal aquifer of Bonifacio (Corsica, France). *Sci. Total Environ.* 573, 233–246.
 1106 <https://doi.org/10.1016/j.scitotenv.2016.08.087>
 1107 Schildgen, T.F., Cosentino, D., Frijia, G., Castorina, F., Dudas, F.O., Iadanza, A.,
 1108 Sampalmieri, G., Cipollari, P., Caruso, A., Bowring, S.A., M. R. Strecker, 2014. Sea
 1109 level and climate forcing of the Sr isotope composition of late Miocene Mediterranean
 1110 marine basins. *Geochemistry, Geophys. Geosystems* 15, 4692–4711.
 1111 <https://doi.org/10.1002/2014GC005332>
 1112 Sessa, J.A., Ivany, L.C., Schlossnagle, T.H., Samson, S.D., Schellenberg, S.A., 2012. The
 1113 fidelity of oxygen and strontium isotope values from shallow shelf settings : Implications
 1114 for temperature and age reconstructions. *Palaeogeogr. Palaeoclimatol. Palaeoecol.* 342–
 1115 343, 27–39. <https://doi.org/10.1016/j.palaeo.2012.04.021>
 1116 Shao, Y., Farkaš, J., Holmden, C., Mosley, L., Kell-Duivestien, I., Izzo, C., Reis-Santos, P.,
 1117 Tyler, J., Törber, P., Frýda, J., Taylor, H., Haynes, D., Tibby, J., Gillanders, B.M., 2018.
 1118 Calcium and strontium isotope systematics in the lagoon-estuarine environments of

1119 South Australia: Implications for water source mixing, carbonate fluxes and fish
 1120 migration. *Geochim. Cosmochim. Acta* 239, 90–108.
 1121 <https://doi.org/10.1016/j.gca.2018.07.036>
 1122 Sharma, M., Balakrishna, K., Hofmann, A.W., Shankar, R. 2007. The transport of Osmium
 1123 and Strontium isotopes through a tropical estuary. *Geochimica et Cosmochimica Acta*,
 1124 71, 4856–4867. <https://doi.org/10.1016/j.gca.2007.08.004>
 1125 Stein, M., Starinsky, A., Agnon, A., Katz, A., Raab, M., Spiro, B., Zak, I., 2000. The impact
 1126 of brine-rock interaction during marine evaporite formation on the isotopic Sr record in
 1127 the oceans. Evidence from Mt. Sedom, Israel. *Geochim. Cosmochim. Acta* 64(12),
 1128 2039–2053. [https://doi.org/10.1016/S0016-7037\(00\)00370-7](https://doi.org/10.1016/S0016-7037(00)00370-7)
 1129 Stieglitz, T.C., van Beek, P., Souhaut, M., Cook, P.G., 2013. Karstic groundwater discharge
 1130 and seawater recirculation through sediments in shallow coastal Mediterranean lagoons,
 1131 determined from water, salt and radon budgets. *Sci. Rep.* 8, 73–84.
 1132 <https://doi.org/10.1016/j.marchem.2013.05.005>
 1133 Tachikawa, K., Roy-Barman, M., Michard, A., Thouron, D., Yeghicheyan, D., Jeandel, C.,
 1134 2004. Neodymium isotopes in the Mediterranean Sea: Comparison between seawater and
 1135 sediment signals. *Geochemical et Cosmochimica Acta*, 68(14), 3095–3106.
 1136 Takada, H., Tagami, K., Aono, T., Uchida, S., 2014. Distribution coefficients (K_d) of
 1137 strontium and significance of oxides and organic matter in controlling its partitioning in
 1138 coastal regions of Japan. *Science of the Total Environment*, 490, 979–986.
 1139 Tanhua, T., Hainbucher, D., Schroeder, K., Cardin, V., Álvarez, M., Civitarese, G., 2013. The
 1140 Mediterranean Sea system: A review and an introduction to the special issue. *Ocean Sci.*
 1141 9, 789–803. <https://doi.org/10.5194/os-9-789-2013>
 1142 Tartinville, B., Deleersnijder, E., Rancher, J., 1997. The water residence time in the Mururoa
 1143 atoll lagoon: Sensitivity analysis of a three-dimensional model. *Coral Reefs* 16, 193–203.

1144 <https://doi.org/10.1007/s003380050074>

1145 Teichert, B.M.A., Chevalier, N., Gussone, N., Bayon, G., Ponzevera, E., Ruffine, L., Strauss,
 1146 H., 2018. Sulfate-dependent anaerobic oxidation of methane at a highly dynamic
 1147 bubbling site in the Eastern Sea of Marmara (Çınarcık Basin). *Deep. Res. Part II Top.*
 1148 *Stud. Oceanogr.* 153, 79–91. <https://doi.org/10.1016/j.dsr2.2017.11.014>

1149 Trezzi, G., Garcia-Orellana, J., Rodellas, V., Masqué, P., Garcia-Solsona, E., Andersson, P.S.,
 1150 2017. Assessing the role of submarine groundwater discharge as a source of Sr to the
 1151 Mediterranean Sea. *Geochim. Cosmochim. Acta* 200, 42–54.
 1152 <https://doi.org/10.1016/J.GCA.2016.12.005>

1153 Uddin, S., Al Ghadban, A.N., Behbahani, M., 2013. Baseline concentrations of strontium and
 1154 ^{90}Sr in seawater from the northern Gulf. *Marine Pollution Bulletin*, 75 (1-2), 301-304.
 1155 <https://doi.org/10.1016/j.marpolbul.2013.06.042>

1156 Umgiesser, G., Ferrarin, C., Cucco, A., De Pascalis, F., Bellafore, D., Ghezzi, M., Bajo, M.,
 1157 2014. Comparative hydrodynamics of 10 Mediterranean lagoons by means of numerical
 1158 modeling. *J. Geophys. Res. Oceans.* 119 (4), 2212–2226.
 1159 <https://doi.org/10.1002/2013JC009512>

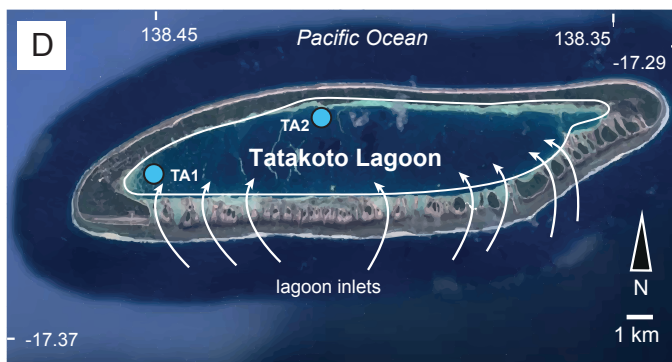
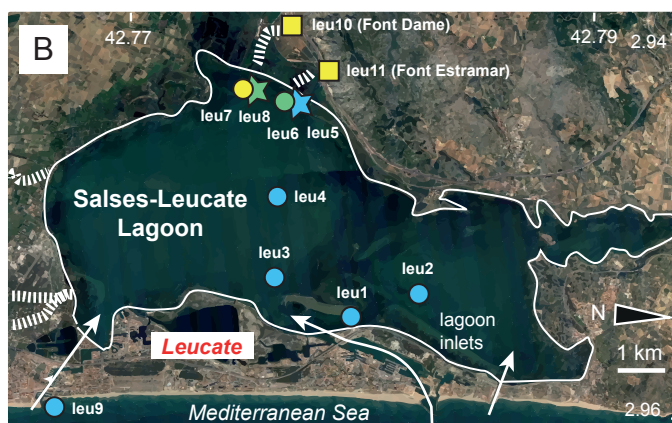
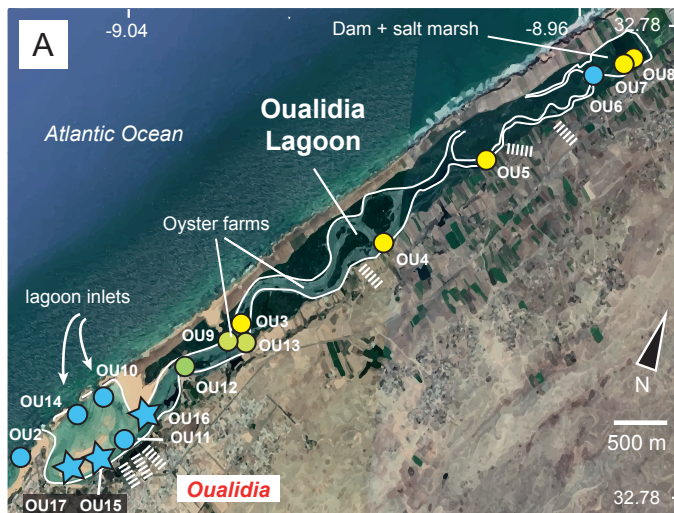
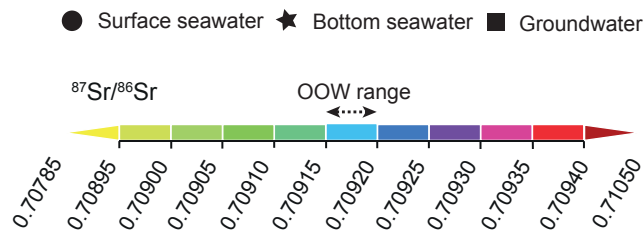
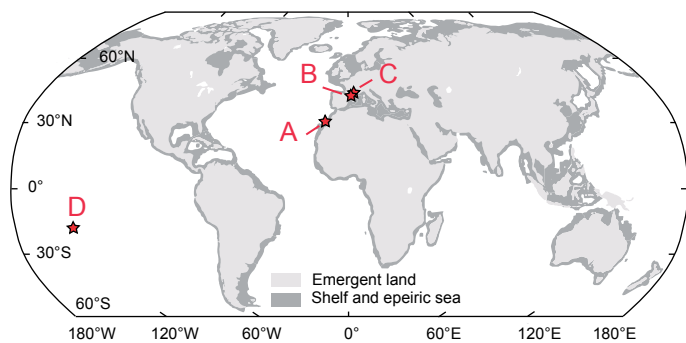
1160 Ünlüata, U., Oguz, T., Latif, M.A., Özsoy, E., 1990. On the physical oceanography of the
 1161 Turkish straits. In: Pratt, L.J. (ed.) *The Physical oceanography of sea straits*, NATO/ASI
 1162 series, pp 25-60. Kluwer Academic Publishers

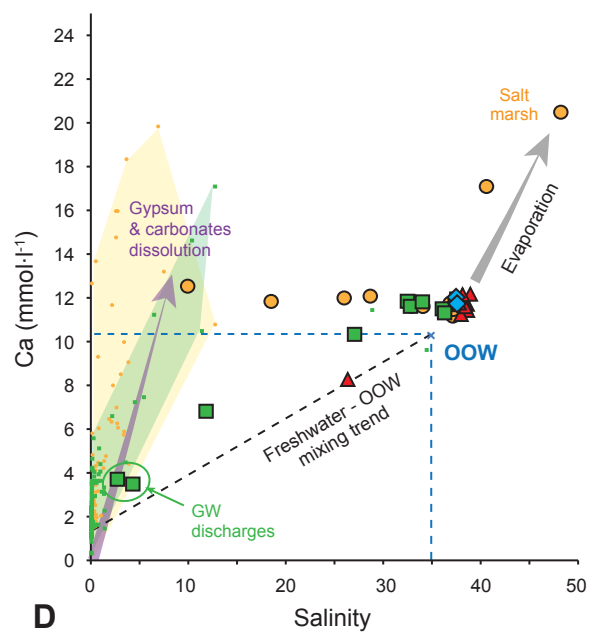
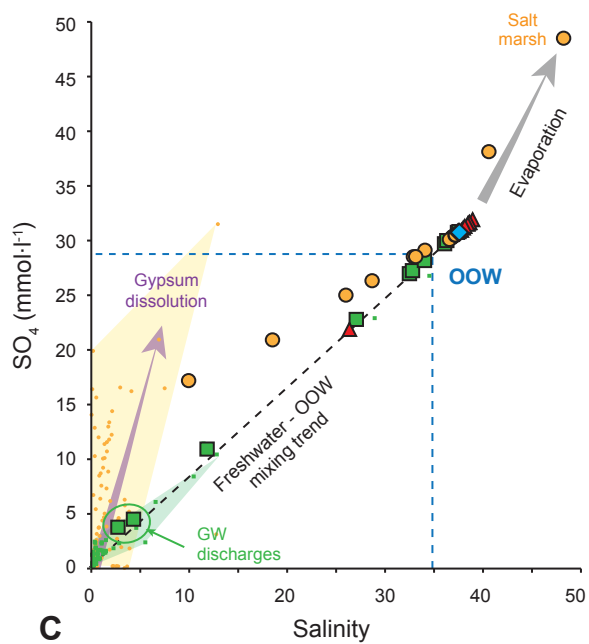
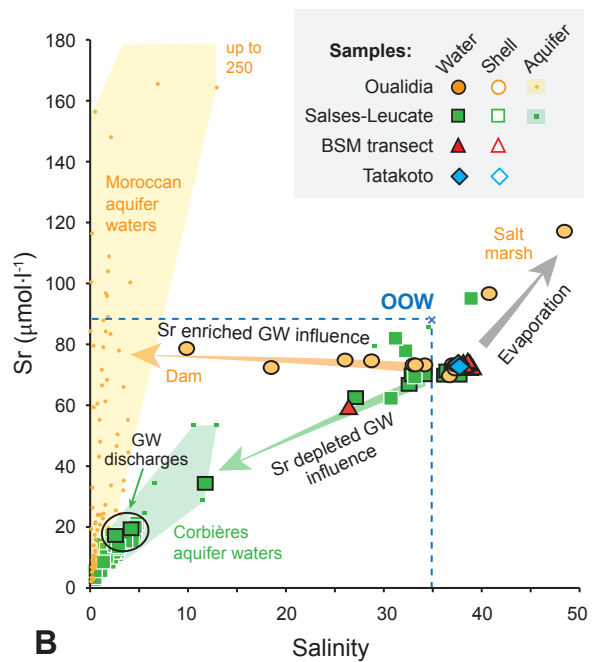
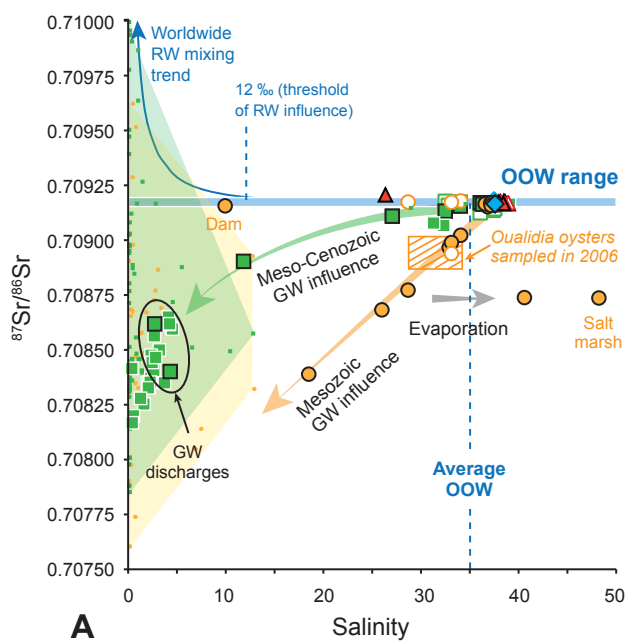
1163 Van Wynsberge, S., Menkes, C., Le Gendre, R., Passfield, T., Andréfouët, S., 2017. Are Sea
 1164 Surface Temperature satellite measurements reliable proxies of lagoon temperature in the
 1165 South Pacific? *Estuar. Coast. Shelf Sci.* 199, 117–124.
 1166 <https://doi.org/10.1016/J.ECSS.2017.09.033>

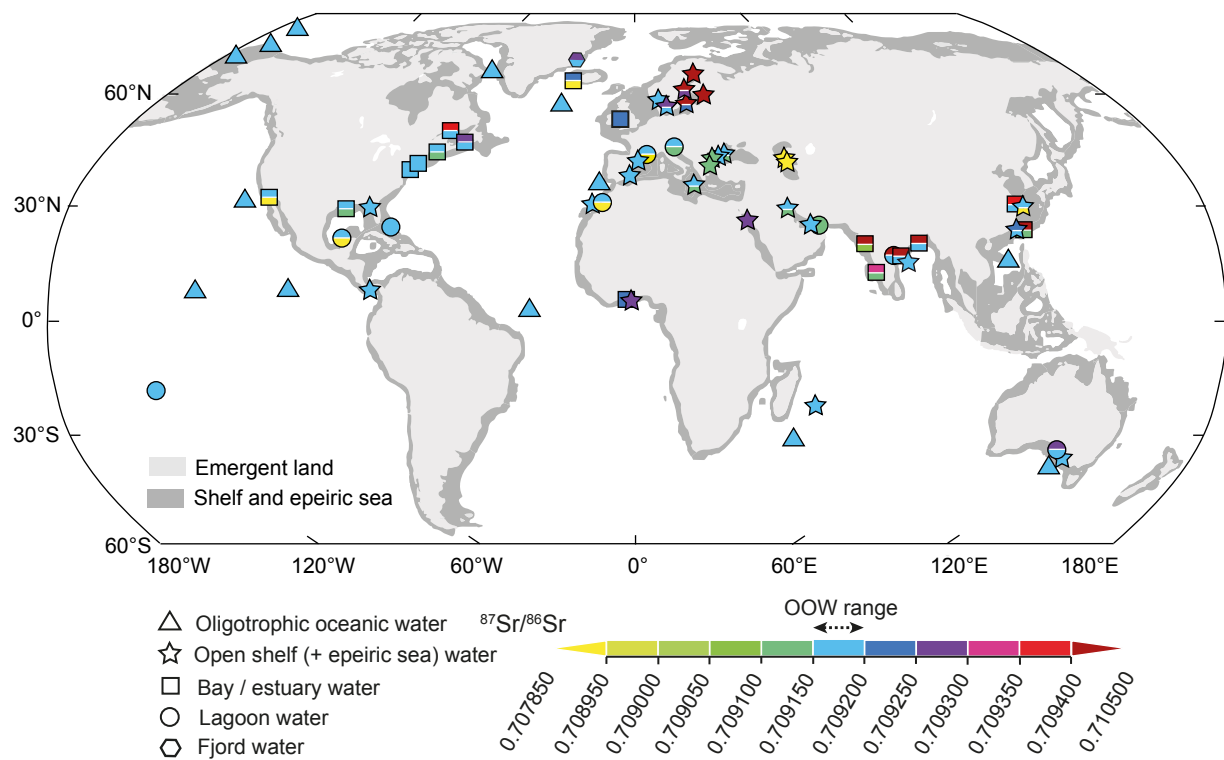
1167 Veizer, J., 1989. Strontium isotopes in seawater through time. *Annu. Rev. Earth Planet. Sci.*
 1168 17, 141–167.

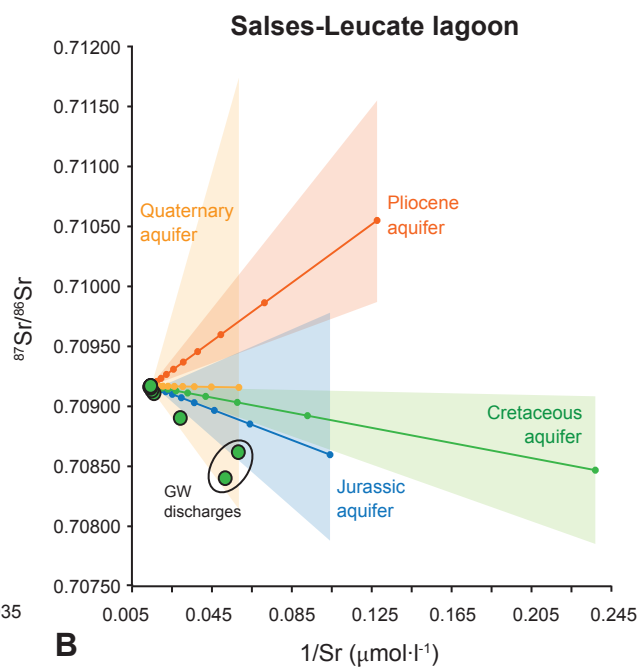
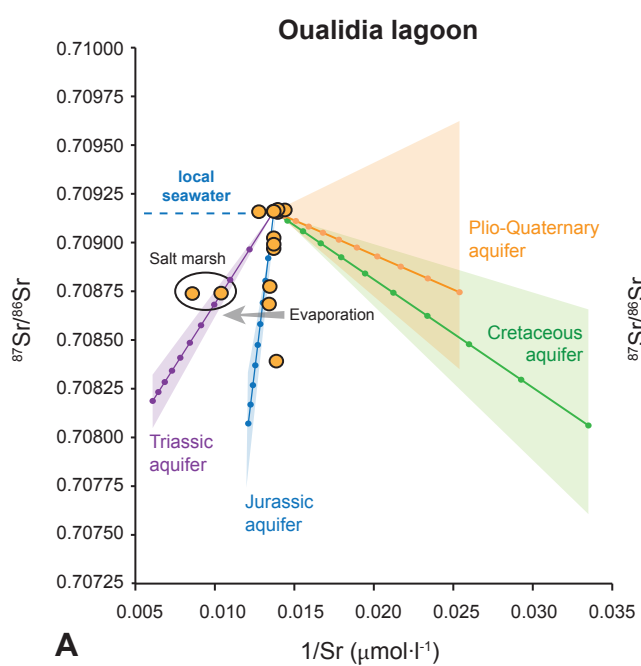
1169 Vinson, D.S., Tagma, T., Bouchaou, L., Dwyer, G.S., Warner, N.R., 2013. Applied
 1170 Geochemistry Occurrence and mobilization of radium in fresh to saline coastal
 1171 groundwater inferred from geochemical and isotopic tracers. *Appl. Geochemistry* 38,
 1172 161–175. <https://doi.org/10.1016/j.apgeochem.2013.09.004>
 1173 Waljeski, C., 2003. Systematic karst pool erosion within the conglomerate platforms of
 1174 Moorea, French Polynesia. *Biol. Geomorphol. Trop. Islands* 12, 117–128.
 1175 Wang, Z., Liu, C., Han, G., Xu, Z. 2001. Strontium isotopic geochemistry of the Changjiang
 1176 estuarine waters: Implication for water-sediment interaction. *Science in China (Series E)*,
 1177 44, 129-133. <https://doi.org/10.1007/BF02916803>
 1178 Wang, R.M., You, C.F., 2013. Uranium and strontium isotopic evidence for strong submarine
 1179 groundwater discharge in an estuary of a mountainous island: A case study in the
 1180 Gaoping River Estuary, Southwestern Taiwan. *Mar. Chem.* 157, 106–116.
 1181 <https://doi.org/10.1016/j.marchem.2013.09.004>
 1182 Wierzbowski, H., Anczkiewicz, R., Bazarnik, J., Pawlak, J., 2012. Strontium isotope
 1183 variations in Middle Jurassic (Late Bajocian–Callovian) seawater: Implications for
 1184 Earth's tectonic activity and marine environments. *Chem. Geol.* 334, 171–181.
 1185 <https://doi.org/10.1016/J.CHEMGEO.2012.10.019>
 1186 Winter, B.L., Johnson, C.M., Clark, D.L., 1997. Strontium, neodymium, and lead isotope
 1187 variations of authigenic and silicate sediment components from the Late Cenozoic Arctic
 1188 Ocean: Implications for sediment provenance and the source of trace metals in seawater.
 1189 *Geochim. Cosmochim. Acta* 61, 4181–4200. [https://doi.org/10.1016/S0016-](https://doi.org/10.1016/S0016-7037(97)00215-9)
 1190 [7037\(97\)00215-9](https://doi.org/10.1016/S0016-7037(97)00215-9)
 1191 Xu, Y., Marcantonio, F. 2007. Strontium isotope variations in the lower Mississippi River and
 1192 its estuarine mixing zone. *Marine Chemistry*, 105, 118-128.
 1193 <https://doi.org/10.1016/j.marchem.2007.01.004>

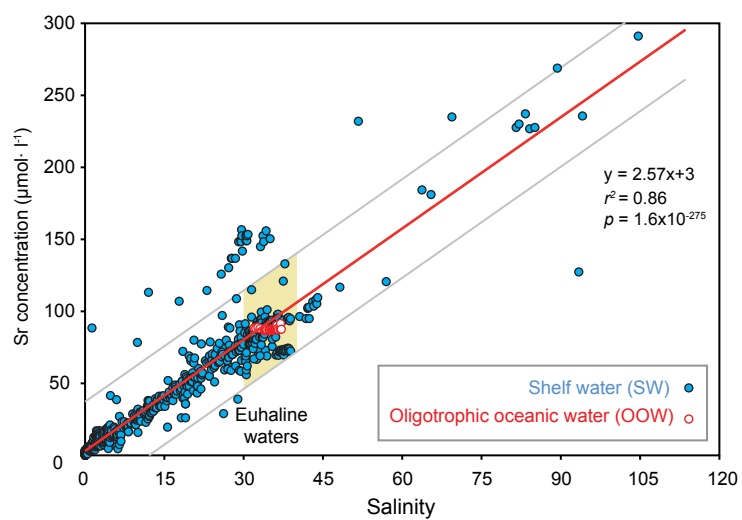
1194 Zaky, A.H., Brand, U., Buhl, D., Blamey, N., Bitner, M.A., Logan, A., Gaspard, D., Popov,
1195 A., 2018. Strontium isotope geochemistry of modern and ancient archives: tracer of
1196 secular change in ocean chemistry. *Can. J. Earth Sci.* 56, 245–264.
1197 <https://doi.org/10.1139/cjes-2018-0085>
1198











Studied site	Sample	Water type (environment)	Water depth (mbsl)	Salinity	Ca mmol·l ⁻¹	Mg mmol·l ⁻¹	Na mmol·l ⁻¹	K mmol·l ⁻¹	SO ₄ mmol·l ⁻¹	Cl mmol·l ⁻¹	Li μmol·l ⁻¹	Br μmol·l ⁻¹	Sr μmol·l ⁻¹	⁸⁷ Sr/ ⁸⁶ Sr	2 std dev
Oualidia lagoon, Morocco	OU2	Atlantic seawater (beach)	0	37.2	11.47	59.23	567	9.97	30.51	581	48.72	865	73.0	0.709158	0.000004
	OU3	Lagoon water	0	28.7	12.08	47.85	453	7.83	26.33	448	36.26	667	74.4	0.708772	0.000004
	OU4	Lagoon water	0	26.0	11.99	42.47	399	6.96	25.01	406	31.53	597	74.6	0.708682	0.000004
	OU5	Lagoon water	0	18.5	11.84	30.88	276	4.85	20.92	289	23.17	420	72.2	0.708389	0.000004
	OU6	Lagoon water (close to the dam)	0	9.9	12.53	18.48	138	2.60	17.19	155	15.85	223	78.4	0.709156	0.000004
	OU7	Lagoon water (salt marsh)	0	40.6	17.09	71.32	653	11.55	38.13	634	54.53	1012	96.4	0.708738	0.000004
	OU8	Lagoon water (salt marsh)	0	48.2	20.49	92.47	753	15.36	48.51	753	80.57	1302	116.8	0.708736	0.000004
	OU9	Lagoon water	0	33.1	11.83	53.14	535	9.37	28.53	517	42.62	768	73.0	0.708989	0.000004
	OU10	Lagoon water	0	37.1	11.16	57.34	586	10.08	30.49	580	47.44	862	71.7	0.709168	0.000004
	OU11	Lagoon water	0	36.6	11.38	58.32	580	10.09	30.10	571	45.66	862	69.5	0.709165	0.000004
	OU12	Lagoon water	0	34.1	11.60	53.28	542	9.34	29.12	532	43.26	786	73.0	0.709022	0.000004
	OU13	Lagoon water	0	32.9	11.61	52.32	524	9.04	28.53	514	41.77	762	73.0	0.708967	0.000004
	OU14	Lagoon water	0	37.0	11.54	58.44	591	10.41	30.38	578	48.10	856	72.1	0.709162	0.000004
	OU15	Lagoon water	3	37.1	11.34	57.23	598	10.20	30.47	579	49.57	855	71.8	0.709164	0.000004
	OU16	Lagoon water	3	36.8	11.51	57.00	601	10.22	30.26	575	46.99	846	71.7	0.709152	0.000004
Salses-Leucate lagoon, France	OU17	Lagoon water	3	36.9	11.76	58.65	600	10.26	30.35	576	47.06	833	73.1	0.709159	0.000004
	LEU9	Mediterranean seawater (beach)	0	37.6	11.95	61.04	598	10.71	30.82	586	46.71	871	69.7	0.709170	0.000004
	LEU1	Lagoon water (mussel farm)	0.5	36.3	11.31	57.40	577	10.24	30.00	567	45.72	848	71.0	0.709164	0.000004
	LEU2	Lagoon water	0	36.1	11.50	57.25	579	10.39	29.71	563	46.54	849	69.7	0.709170	0.000004
	LEU3	Lagoon water	0	37.4	11.69	59.52	593	10.61	30.75	584	47.81	880	71.9	0.709161	0.000004
	LEU4	Lagoon water	0	34.0	11.82	56.83	576	9.95	28.17	531	42.88	786	69.8	0.709155	0.000004
	LEU5	Lagoon water	1.5	32.8	11.61	54.76	553	9.65	27.25	512	39.48	762	69.8	0.709169	0.000004
	LEU6	Lagoon water	0	32.5	11.85	54.75	556	9.67	26.97	507	41.36	746	66.7	0.709132	0.000004
	LEU7	Lagoon water	0	11.8	6.82	20.23	186	3.25	10.93	185	11.42	235	34.2	0.708903	0.000004
	LEU8	Lagoon water	2.5	27.1	10.33	44.94	454	7.73	22.79	422	30.55	618	62.3	0.709109	0.000004
Banyuls-sur-Mer transect, France	LEU11	Groundwater (Font Estramar discharge)	0	4.3	3.49	6.83	39	1.07	4.52	67	4.78	86	19.3	0.708401	0.000004
	LEU10	Groundwater (Font Dame discharge)	0	2.7	3.71	4.37	9	0.62	3.78	42	2.77	51	17.2	0.708618	0.000004
	BA1	Mediterranean seawater (open shelf)	22	38.1	12.15	60.73	622	10.57	31.29	595	45.09	894	73.1	0.709174	0.000004
	BA2	Mediterranean seawater (open shelf)	0	37.8	11.76	58.50	602	10.25	30.94	590	48.45	884	72.7	0.709167	0.000004
	BA3	Mediterranean seawater (open shelf)	40	38.4	11.60	59.69	588	10.46	31.49	600	47.76	913	74.5	0.709167	0.000005
	BA4	Mediterranean seawater (open shelf)	0	38.0	11.24	59.91	586	10.33	31.14	593	45.55	893	74.0	0.709173	0.000004
	BA5	Mediterranean seawater (open shelf)	140	38.6	11.43	59.52	579	10.40	31.66	603	50.66	900	73.9	0.709170	0.000004
	BA6	Mediterranean seawater (open shelf)	0	38.5	11.75	60.35	594	10.60	31.58	601	49.11	914	73.6	0.709176	0.000004
	BA7	Mediterranean seawater (open shelf)	510	38.9	12.17	63.26	615	11.19	31.91	608	49.62	904	72.4	0.709166	0.000004
	BA8	Mediterranean seawater (open shelf)	0	38.6	11.71	60.22	612	10.75	31.64	603	47.38	911	72.2	0.709174	0.000004
Tatakoto lagoon, French Polynesia	BA9	Mediterranean seawater (beach)	0	26.4	8.27	42.21	432	7.40	21.87	412	30.34	605	59.3	0.709206	0.000004
	T1	Lagoon water	2	37.6	11.73	61.81	599	10.84	30.75	587	50.84	889	72.4	0.709165	0.000004
Global ocean#	T2	Lagoon water	2	37.5	12.02	62.77	619	11.16	30.75	585	50.03	887	73.5	0.709171	0.000004
	-	Oligotrophic Oceanic water (OOW)	-	34.9	10.28	54.10	468	10.21	28.30	545	24.6	873	88.0	0.709172	0.000023

Studied site	Shell sample	Corresponding water sample	Species	Ca (mg·g ⁻¹)	Mg (µg·g ⁻¹)	Sr (µg·g ⁻¹)	⁸⁷ Sr/ ⁸⁶ Sr	2 std dev
Oualidia lagoon, Morocco	O 1	OU 3	<i>Crassostrea gigas</i>	370	3888	1091	0.709174	0.000004
	O 2	OU 9	<i>Crassostrea gigas</i>	371	1361	575	0.709173	0.000004
	O 3	OU 12	<i>Venerupis decussata</i>	334	118	1689	0.709179	0.000004
	O 4	OU 9	<i>Solen marginatus</i>	361	268	2797	0.708939	0.000004
Salses-Leucate lagoon, France	S1	LEU 9	<i>Mytilus galloprovincialis</i>	354	483	746	0.709143	0.000004
	S2	LEU 2	<i>Glycymeris glycymeris</i>	na	na	na	0.709125	0.000004
	S3	LEU 3	<i>Crassostrea sp.</i>	na	na	na	0.709136	0.000004
	S4	LEU 4	<i>Mytilus galloprovincialis</i>	364	945	969	0.709174	0.000004
	S5	LEU 5	<i>Mytilus galloprovincialis</i>	378	1291	932	0.709158	0.000004
	S6	LEU 6	<i>Mytilus galloprovincialis</i>	349	135	1511	0.709177	0.000004
Banyuls-sur-Mer, France	Bs 1	B 1	Bivalve fragments	360	792	1513	0.709174	0.000004
	Bs 2	B 3	<i>Turritella communis</i>	362	413	1645	0.709173	0.000004
	Bs 3	B 5	Bivalve fragments	na	na	na	0.709165	0.000004
	Bs 4	B 7	Bivalve fragments	381	11554	2214	0.709171	0.000004
Tatakoto lagoon, French Polynesia	Ts 1	T1	<i>Tridacna maxima</i>	na	na	na	0.709178	0.000004
	Ts 2	T1	<i>Tridacna maxima</i>	365	810	1587	0.709164	0.000004
	Ts 3	T2	<i>Tridacna maxima</i>	na	na	na	0.709182	0.000004
	Ts 4	T2	<i>Tridacna maxima</i>	357	205	1644	0.709172	0.000004

Studied sites	End-members	Water type	Average Sr ($\mu\text{mol}\cdot\text{l}^{-1}$)	Minimal Sr ($\mu\text{mol}\cdot\text{l}^{-1}$)	Maximal Sr ($\mu\text{mol}\cdot\text{l}^{-1}$)	Average $^{87}\text{Sr}/^{86}\text{Sr}$	Minimal $^{87}\text{Sr}/^{86}\text{Sr}$	Maximal $^{87}\text{Sr}/^{86}\text{Sr}$	References
Morocco	Plio-Quaternary aquifer	GW	39.4	1.4	148.0	0.70874	0.70835	0.70962	Fakir et al., 2002; Kaid Rassou et al., 2005; Vinson et al., 2006
	Cretaceous aquifer	GW	29.8	3.0	116.4	0.70760	0.70760	0.70866	Fakir et al., 2002; Fadili et al., 2015; Bouchaou et al., 2017
	Jurassic aquifer	GW	82.7	36.3	249.9	0.70807	0.70774	0.70833	Kaid Rassou et al., 2005; Bouchaou et al., 2017
	Triassic aquifer	GW	164.9	164.4	165.5	0.70819	0.70805	0.70832	Bouchaou et al., 2017
	Atlantic water at Oualidia	SW	73.0	-	-	0.70916	-	-	<i>this study</i>
Corbières region, France	Quaternary aquifer	GW	17.1	1.8	85.5	0.70916	0.70814	0.71174	Petelet et al., 1998; Petelet-Giraud et al., 2016
	Pliocene aquifer	GW	7.8	4.7	15.2	0.71055	0.70987	0.71155	Petelet-Giraud et al., 2016
	Cretaceous aquifer	GW	4.2	1.2	9.0	0.70847	0.70753	0.70908	Khaska et al., 2013
	Jurassic aquifer	GW	9.6	0.3	53.0	0.70860	0.70788	0.70978	Aquilina et al., 2003; Petelet-Giraud et al., 2016
	Mediterranean water at Salses-Leucate	SW	69.7	-	-	0.70917	-	-	<i>this study</i>

